Title
Vehicle Modeling And Control For Automated Highway Systems

Authors
Hedrick, J. K.
Mcmahnon, D. H.
Swaroop, D.

Publication Date
1993

CALIFORNIA PATH PROGRAM
INSTITUTE OF TRANSPORTATION STUDIES
UNIVERSITY OF CALIFORNIA, BERKELEY

Vehicle Modeling and Control for Automated Highway Systems

J. K Hedrick, D.H. McMahon, D. Swaroop

Longitudinal Contrtol Group
University of California, Berkeley

UCB-ITS-PRR-93-24

This work was performed as part of the California PATH Program of the University of California, in cooperation with the State of California Business, Transportation, and Housing Agency, Department of Transportation; and the United States Department Transportation, Federal Highway Administration.

NOVEMBER 1993

ISSN 1055-1425

Table of Contents

Abstract

1. Introduction 3

2. Vehicle Modeling & Validation

2.1 Complex Vehicle Model 6
2.1.1. Engine Model 7
2.1.2. Transmission Model 11
2.1.3. Drivetrain Model 12
2.2. Three State Vehicle Model 18
2.3. Four State Vehicle Model 20
2.4. Model Validation 22

3. Platoon Control Algorithms for IVHS

3.1 Three State Longitudinal Controller Design 24
3.1.1. Sliding Controller Design 26
3.1.2. I/O Linearization Controller Design 28
3.1.3. Controller Equivalence Conditions 32
3.2 Headway Longitudinal Controller Design 33

4. Longitudinal Platoon Control: Simulation Results

4.1 Complex Vehicle Model: Spacing Control 36
4.2 Four State Vehicle Model: Spacing Control 39
4.3 Three State Vehicle Model: Headway Control 41

5. Implementation Issues

5.1 Actuator Specifications 46

5.2 Brake Actuator Control and Testing 51

6. Experimental Platoon Development

6.1 Integrated Platoon Control System (IPCS) 55

6.2 The Operating Environment 57

6.3 IPCS Experimental Results

6.3.1. Two Car Platoon Testing 58

6.3.2. Four Car Platoon Testing 62

7. Conclusions 66

Acknowledgement 68

References 69

ABSTRACT

This report summarizes recent work done in the area of longitudinal control of a platoon of autonomous vehicles. As a prerequisite to controller design, a twelve state nonlinear model including an internal combustion engine, engine transmission dynamics, and tire friction characteristics has been developed. Using certain physical assumptions, we present two simplified models for simulation and controller design. After outlining the control problem, we propose two platooning strategies based on spacing or headway criterion. To solve the control requirements, decentralized nonlinear control strategies using throttle angle and brake torque control for a platoon were developed using a modification of the technique of *Sliding Control* and Input-Output Linearization. In our analysis, the quantities of primary concern are position and velocity tracking errors. Simulation results on multiple vehicle platoons demonstrate excellent tracking using the spacing-based controllers. The use of headway based controllers produced degraded performance as compared to the spacing based controllers. The control strategies were implemented experimentally on the Integrated Platoon Control System (IPCS) during two and four car platoon testing.

Chapter 1
Introduction

Over the past three decades Intelligent Vehicle Highways Systems (IVHS) have become a topic of considerable interest. Such systems have been developed as a safe and efficient means of travel on congested roadways. Recent advances in technology have facilitated the development of the necessary components of an IVHS. Computer systems, communication systems, optical systems and sensors have improved significantly in the areas of speed, accuracy, and repeatability. Given the breadth of these technological advances the term "IVHS" is one describing a variety of devices/systems. These systems range from traffic management systems to control traffic flow, to autonomous vehicular systems. The California Partners for Advanced Transit and Highways (PATH) has been developing advanced vehicle control systems (AVCS). These systems control the longitudinal and lateral motions of all vehicles in a vehicle-follower or platoon system. This report summarizes work

done in the area of Longitudinal Control as part of the PATH project.

Chapter 2 describes several vehicle models used for simulation and controller design. The vehicle models are based upon the FORD Lincoln Town Car which is the experimental vehicle. Firstly, a complex vehicle model of consisting of twelve states was developed. These states are distributed among the three main vehicle modules: the engine, transmission, and drivetrain. Several physical assumptions are made to simplify the mathematical modeling. Using these assumptions three and four state vehicle models excluding and including tire slip dynamics, respectively, were developed. Validation studies were then conducted on the resulting four state vehicle model.

Chapter 3 examines two different IVHS control strategies: spacing control and headway control. Using the three state simplified model, we present two spacing controller designs. The control design methodologies known as *Sliding Control* and I/O Linearization were chosen for their specific application to nonlinear systems. A modification of the sliding technique which uses multiple *sliding surfaces* was used for this application. The resulting control scheme produces both throttle and brake command signals. The alternative design scheme for a constant-headway controller is also developed using the multiple surface approach.

In Chapter 4 the controllers based upon the three state model were used to study a typical tracking maneuver under ideal road conditions and perfect knowledge of the vehicle plant. Simulation results of a platoon of ten vehicles using both the complex model vehicle as well as the simplified three state vehicle are provided.

The control scheme developed for this application produces two control outputs, a throttle and brake command. Chapter 5 addresses the implementation issues

relevant to these controls. Simulations were used to determine the minimum specifications for the throttle and brake actuators. A description of the brake system hardware used to generate the control input to the brake actuator is provided. The input-output characteristic of the total brake system is also documented.

In chapter 6 the development of the experimental platoon system is summarized. The various components of the Integrated Platoon Control System (IPCS) are described along with the operating environment and the error checking and safety features. Experimental results using the IPCS for multi-vehicle platoons are also shown.

Chapter 2
Vehicle Modeling & Validation

2.1 Complex Vehicle Model

In order to facilitate the development of a longitudinal controller for platoon purposes a model of a vehicle's longitudinal dynamics was necessary. The purpose of this model was twofold. Firstly, a simulation model was needed to accurately describe the highly nonlinear dynamics of an automobile. It was used to test the various control schemes before experimental implementation. Thus we can minimize the number of problems encountered during experimental field testing. Secondly, the control design technique chosen for the problem requires a knowledge of the vehicle plant dynamics.

The automotive power-train was partitioned into the following segments: an engine, a transmission (including a torque converter), a drivetrain (including rubber

tires), and all other components that can influence the longitudinal performance of an automobile (such as throttle, fuel control, spark control, EGR system, clutches, bands, brakes, accessories, etc.).

The mathematical model developed here is based on tabulated data for a 1990 Ford Lincoln Town car. The basic modeling was adopted from a model of a typical front wheel drive vehicle equipped with a V-6 engine developed by Moskwa and Hedrick [9] and Cho and Hedrick [4]. The model includes twelve state variables: four for the engine, two for the transmission, and six for the drivetrain, plus two time delays associated with the engine.

2.1.1 Engine Model

A continuous four stroke spark ignition engine based on the model developed by Moskwa and Hedrick [9] is presented below. The four engine state variables are: the pressure in the intake manifold, the exhaust gas recirculation rate, the engine speed, and the mass flow rate of fuel entering the combustion chamber. The engine modelled below is a 5.0 liter V-S engine.

The state equation for the pressure in the intake manifold is given by:

$$\dot{P}_m = \left\{ \left(\frac{\dot{T}_m}{T_m} \right) - c\ \omega_e \eta_{vol} \right\} P_m + \left\{ \frac{RT_m}{V_m} \right\} \cdot \left(\dot{m}_{ai} + \dot{m}_{egri} \right) \qquad (1)$$

where P_m is the manifold pressure, R is the universal gas constant for air, T_m is the manifold temperature, and V_m is the intake manifold volume. The mass rate of air entering the intake manifold is given by:

$$\dot{m}_{ai} = MAX \cdot TC \cdot PRI \qquad (2)$$

The parameter MAX is the maximum flow rate corresponding to a fully open throttle valve. The function ***TC*** is the normalized throttle characteristic, a nonlinear function of the throttle angle a. A piecewise approximation to the function is shown in Figure 1. The function ***PRI*** is a normalized pressure influence function as a function of the pressure ratio $\boldsymbol{PR} = P_m/P_{atm}$, where P_{atm} is atmospheric pressure. The following polynomial approximation may be used instead of the map (see Figure 2):

$$\boldsymbol{PRI} = -4.9958\ PR^5 + 5.8832\ PR^4 - 1.1218\ PR^3 - \boldsymbol{0.6579}\ PR^2 - 0.1278\ \boldsymbol{PR} + 1.0104 \tag{3}$$

The volumetric efficiency, η_{vol}, is known to have the following functional dependence:

$$\eta_{vol} = \eta_{vol}\ (P_m, \omega_e)$$

where ω_e is the engine speed. The mass of air in the intake manifold, m_a, is calculated from the ideal gas law

$$m_a = \frac{M_{air} V_m}{R\ T_m}\ P_m \tag{4}$$

where M_{air} is the molecular weight of air.

The second state variable, associated with the intake manifold, is the mass flow rate of exhaust gas out of the intake manifold.

$$\ddot{m}_{egro} = c\ \eta_{vol}\ \omega_e\ (m_{egri} - \dot{m}_{egro}) \qquad Kg/sec^2 \tag{5}$$

where $\dot{m}_{egri}$ is the exhaust gas recirculation rate into the intake manifold.

The third state variable is associated with the fueling rate of the engine. For the sequential-fire port fuel injection system modelled here the state equation is:

$$\tau_f\ \ddot{m}_{fi} + \dot{m}_{fi} = \dot{m}_{fc} \tag{6}$$

where $\dot{m}_{fi}$ is the actual fuel rate entering the combustion chamber and $\dot{m}_{fc}$ is the command fuel rate.

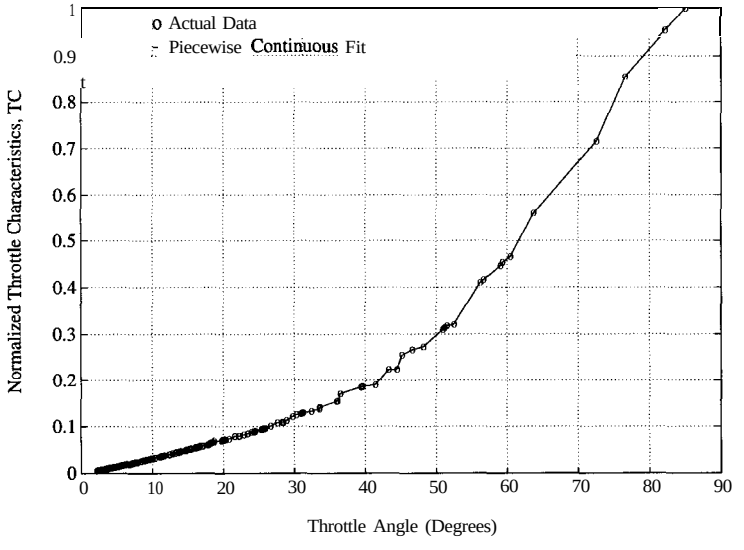

Figure 1: Normalized Throttle Characteristic

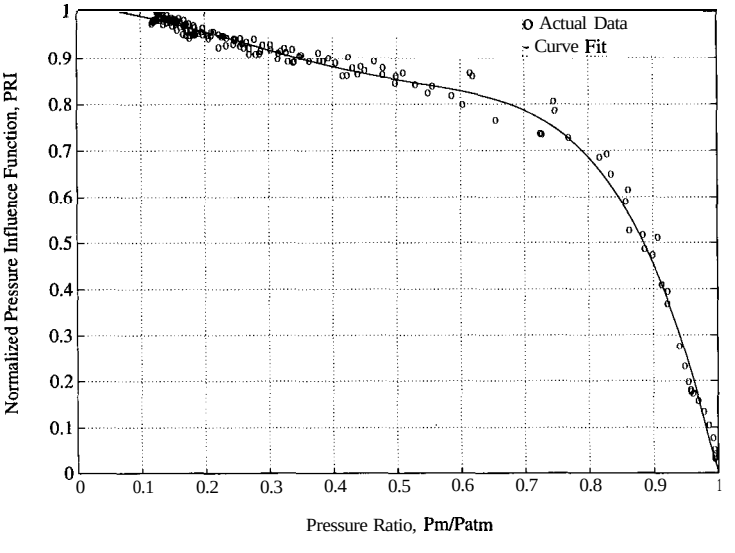

Figure 2: Normalized Pressure Influence Function

The final state variable, associated with torque production, is the engine speed.

It is modelled by:

$$J_e \dot{\omega}_e = T_i - T_f - T_p \tag{7}$$

where J_e is the effective inertia of the engine and torque converter, T_i is the indicated engine torque, T_f is the engine friction torque, and T_p is the torque converter pump torque. The engine torque production is modelled as a continuous time phenomenon.

$$T_i = \frac{c_t \dot{m}_{ao}(t - \Delta t_{it})\ AFI(t - \Delta t_{it})\ SI(t - \Delta t_{st})}{\omega_e(t - \Delta t_{it})} \tag{8}$$

The constant c_t is the maximum torque capability of an engine for a given air mass, engine speed, AFI = 1, and SI = 1. The mass flow rate of air entering the combustion chamber is modelled as:

$$m_{ao} = c_1\ \eta_{vol}\ m_a\ \omega_e \tag{9}$$

The function ***AFZ*** is the normalized air influence function, a nonlinear function of the air to fuel ratio (A/F). The function SI is the normalized spark influence function, a nonlinear function of spark advance from MBT (minimum spark advance for best torque). The time delays associated with the cyclic nature of the engine are At $_{it}$ and ***At,,,*** the intake- to-torque, and spark-to-torque production delays, respectively. The engine friction torque is known to have the following dependence:

$$T_f = T_{fric}(m_{ao},\ \omega_e) \tag{10}$$

In summary, the engine has four state variables ***(P,*** , $\dot{m}_{egro}$, $\dot{m}_{fi}$, and ω_e), three controls (a, ***A/F,*** and ***SA),*** and two time delays A t_{it} and A t_{st} . The parameters for the given engine are given in Table 1.

2.1.2. Transmission Model

2.1.2.1. Torque Converter

The transmission modelled below is an automatic transmission. Therefore included in the modeling are a torque converter, transmission mechanicals, and gear shift capabilities. The torque converter model can be patterned after the nonlinear input-output model developed by Kotwicki (1982). The functional dependencies of the turbine and pump torques are given by:

$$T_{pump} = c_1 \omega_p^2 + c_2 \omega_p \omega_t + c_3 \omega_t^2 \quad (11a)$$

$$T_{turb} = c_4 \omega_p^2 + c_5 \omega_p \omega_t + c_6 \omega_t^2 \quad (11b)$$

where $c_1, \ldots, c_6$ are constant terms. During the high torque transfer phase (converter mode i.e. $\omega_t/\omega_p < 0.9$) the two torque equations are independent. During fluid coupling mode ($\omega_t/\omega_p \geq 0.9$) the two torques are equal and have the following functional dependence.

$$T_{pump} = T_{turb} = c_7 \omega_p^2 + c_8 \omega_p \omega_t + c_9 \omega_t^2 \quad (12)$$

2.1.2.2. Transmission Mechanicals

The transmission mechanicals consist of two interconnected planetary gears and a final drive unit (a single planetary gear). The output of the torque converter (turbine speed) functions as the input to two interconnected planetary gears. The final drive output is connected directly to the driveshaft of the vehicle.

During operation of the transmission in gear there is only one independent state variable, the angular velocity of the turbine. The state equation is:

$$J_{tg}\,\dot{\omega}_t \;=\; T_t - R_g\,R_d\,T_s \tag{13}$$

where J_{tg} is the rotational inertia, R_g is the gear ratio (speed reduction/multiplication) of the respective gear (i.e. g=1, 2, 3, 4) and R_d is the final drive gear ratio. The other state variable, the angular velocity of the reaction carrier (input to final drive unit) is given by:

$$\dot{\omega}_{cr} \;=\; \dot{\omega}_t\,R_g \tag{14}$$

In summary, the transmission has two state variables and no controls. Tabulated values of transmission parameters for a typical automatic transmission equipped with a torque converter are given in Table 1.

2.1.3. Drivetrain Model

The drivetrain model was developed using the bicycle model shown in Figure 3. Included in the model are axle shafts, rubber tires, wheel inertias, and a braking system.

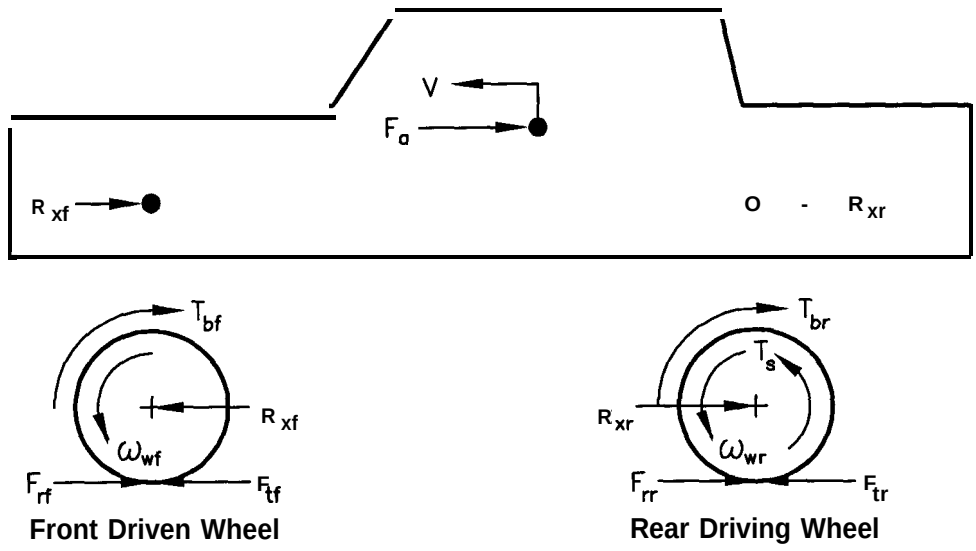

Figure 3: Freebody Diagram of Vehicle Motion

The first drivetrain state variable is the axle shaft torque. The equation of motion is:

$$\dot{T}_s = K_s \, (R_g \, R_d \, \omega_t - \omega_{wr}) \tag{15}$$

where K_s is the left and right axle shaft stiffness combined, and ω_{wr} is the angular velocity of the front wheel.

The state equation for the front wheel is modelled by:

$$J_{wf} \, \dot{\omega}_{wf} = -h_f \, F_{tf} + h_f \, F_{rf} - \varepsilon_f \, N_f - T_{bf} \tag{16}$$

and for the rear wheel by:

$$J_{wr} \dot{\omega}_{wr} = T_s - h_r \, F_{tr} + h_r \, F_{rr} - \varepsilon_r \, N_r - T_{br} \tag{17}$$

where J_{wf} and J_{wr} are the front and rear wheel inertias, respectively, h_f and h_r are the static ground to axle heights of the front and rear wheels, respectively, F_{rf} and F_{rr} are the constant rolling resistances of the front and rear tires respectively, N_f and N_r are the normal loads on the front and rear wheels, respectively, and T_{bf} and T_{br} *are* the front and rear brake torques, respectively. The torque $h_f F_{rf}$ is equal in magnitude to $\varepsilon_f N_f$. Therefore the contribution of these torques to the equation of motion is negated. A similar relation holds for the rear wheel state. The modified front and rear wheel states are:

$$J_{wf} \, \dot{\omega}_{wf} = -h_f \, F_{tf} - T_{bf} \tag{18}$$

$$J_{wr} \dot{\omega}_{wr} = T_s - h_r \, F_{tr} - T_{br} \tag{19}$$

The state variable for the longitudinal motion of the vehicle is:

$$M \, \dot{v} = F_{tf} + F_{tr} - C_a \, V^2 - F_{rf} - F_{rr} \tag{20}$$

where C_a is a constant incorporating the aerodynamic drag coefficient

$(C, \equiv (1/2)\rho\ A\ C,)$.

The tractive/braking forces F_{tf} and F_{tr} result from the deformation of the tire at the tire-ground contact patch. This phenomenon, known as tire slip, is described in detail by Wong (1978). Since tire slip is defined to be a positive quantity, tire slip for a driving torque is given by

$$i_d = 1 - \frac{V}{h\ \omega_w} \tag{21a}$$

and for a braking torque by

$$i_b = 1 - \frac{h\ \omega_w}{V} \tag{21b}$$

where h is the static ground to axle height, ω_w is the angular velocity of the wheel, and V is the vehicle velocity. For small values of tire slip, the tractive/braking force varies linearly with tire slip.

The final two states are the brake torques on the front and rear wheels (left and right sides combined). The brake torques are largely dependent on the braking system. Also, the front to rear brake pressure distribution may be vehicle dependent, especially on those vehicles with anti-lock brakes, traction control systems, etc. The front and rear brake systems on the FORD Lincoln Town Cars are disc types and drum types, respectively (see Figures 4 and 5). The brake torques were modelled with a first order lag expression.

$$\tau_{b,v}\, T_{bf} + T_{bf} = T_{bf,cmd} = K_{bf}\, P_{bf} \tag{22}$$

$$\tau_{b,v}\, T_{br} + T_{br} = T_{br,cmd} = K_{br}\, P_{br} \tag{23}$$

where $\tau_{b,v}$ is the vehicle brake system time constant, K_{bf} is a constant of proportionality between the brake line pressure and the brake torque at the front wheels

(left and right sides combined) and K_{br} is the rear brake proportionality constant. These proportionality constants can be determined from the geometry of the brake system and experimental testing. The pressure distribution is assumed to be evenly split between the front and rear (i.e. $P_{bf} = P_{br} = P_b$).

In summary, the drivetrain has six state variables *(T,,* ω_{wf}, and ω_{wr}, V, T_{bf}, and T_{br}) and one control, P_b. Tabulated values of relevant drivetrain parameters are given for a typical front wheel drive vehicle in Table 1.

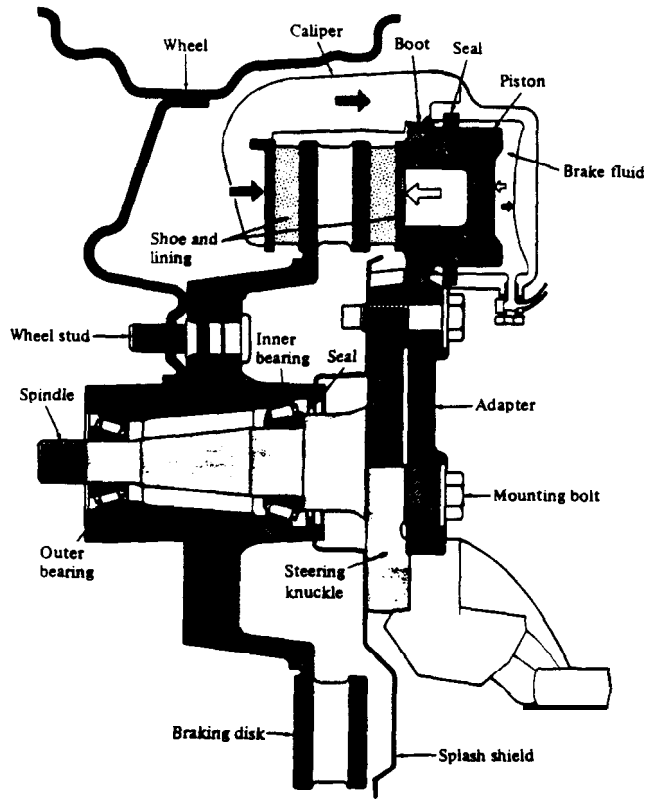

Figure 4: An automotive disk brake (Adopted from Shigley [10])

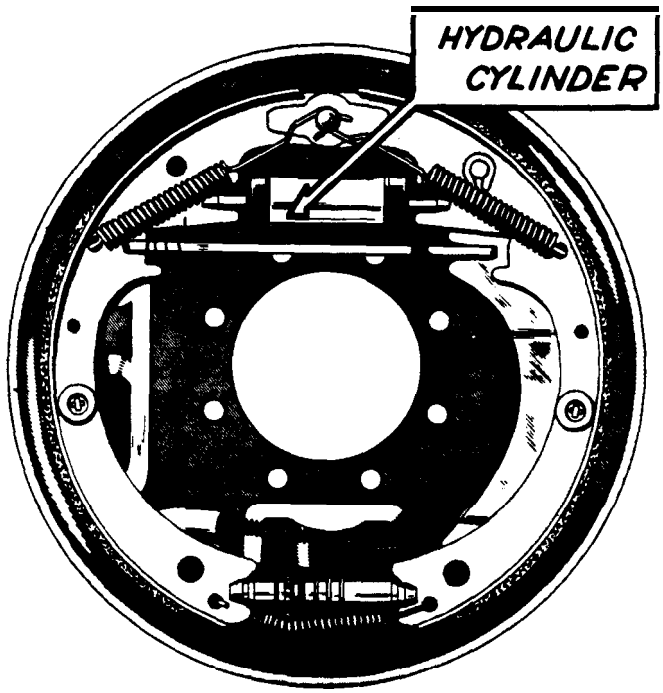

Figure 5: An automotive drum brake (Adopted from White [13])

Table 1: Powertrain Parameters
(All units are in MKS system)

V_e = engine displacement	0.0049 m^3
V_m = intake manifold volume	0.00447 m^3
c_t = engine torque constant	1018686 Nm/kg
J_e = engine & torque converter inertia	0.2630 $kg\ m^2$
MAX = max flow rate into intake manifold	*0.684 kg/s*
A t_{it} = intake to torque production delay	$5.48/\omega_e$
Δt_{st} = spark to torque production delay	$1.30/\omega_e$
τ_f = fuel delivery time constant	0.05 *sec*
R_1 = first gear speed reduction ratio	0.4167
R_2 = second gear speed reduction ratio	0.6817
R_3 = third gear speed reduction ratio	1.0
R_4 = fourth gear speed reduction ratio	1.4993
R_d = final drive speed reduction ratio	0.3058
J_{t1} = effective turbine inertia, 1 stgear	0.08202 $kg\ m^2$
J_{t2} = effective turbine inertia,2ndgear	0.07592 $kg\ m^2$
J_{t3} = effective turbine inertia,3rdgear	0.11388 $kg\ m^2$
J_{t4} = effective turbine inertia,4thgear	0.13150 $kg\ m^2$
J_{wf} = inertia of front wheel	2.565 $kg\ m^2$
J_{wr} = inertia of rear wheel	2.565 $kg\ m^2$
h_f = static axle to ground height of front wheel	0.33 *m*
h_r = static axle to ground height of rear wheel	0.33 *m*
M = vehicle mass	2148 *kg*
K_s = shaft stiffness	*6742 Nm/rad*
F_{rf} = front tire rolling resistance	86.16 N
F_{rr} = rear tire rolling resistance	81.11 N
C_a = aerodynamic drag coefficient	0.53384 *Kg/m*
$Kf(i)$ = tire slip proportionality, front (both sides combined)	83,710 N
$K_r(i)$ = tire slip proportionality, rear (both sides combined)	79,070 N
$\tau_{b,v}$ = Vehicle brake torque time constant	0.1 *sec*
$\tau_{b,t}$ = Total system brake torque time constant	0.25 *sec*
K_{bf} = Front Brake torque proportionality constant	
K_{br} = Rear Brake torque proportionality constant	

2.2. Three State Vehicle Model

In this section we describe a three state vehicle model used for controller design. In this development we make the following assumptions:

(1) time delays associated with power generation in the engine are negligible

(2) the torque converter is locked

(3) no torsion of the drive axle

(4) no slip at the wheels

The states are :

(1) Mass of air in the manifold *(m,)*

(2) Engine speed (ω_e)

(3) Brake torque (T_{br})

(4) Vehicle speed (V)

A free body diagram depicting this simplified model is shown below.

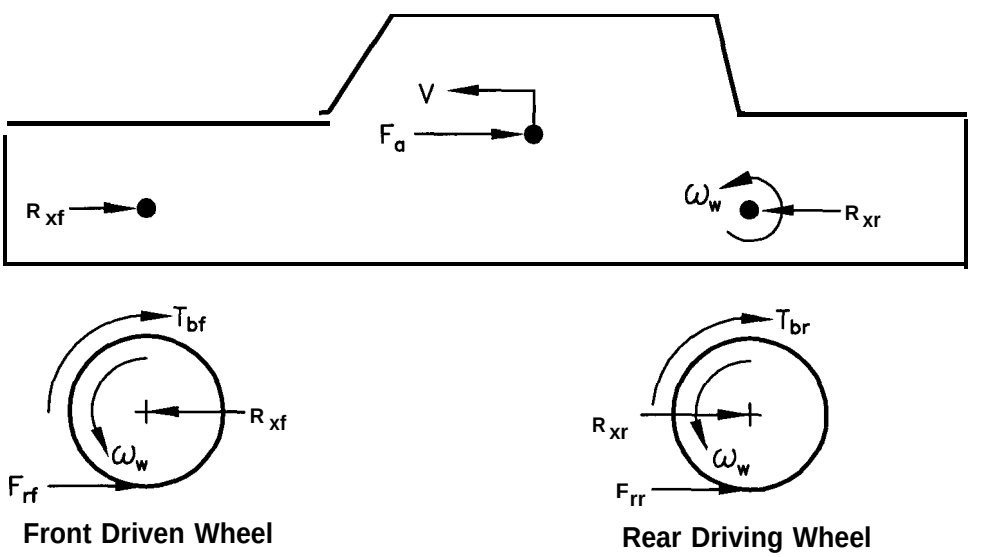

Figure 6: Simplified Freebody Diagram of Vehicle Motion

With these assumptions, the flow of air in the intake manifold is governed by the continuity equation:

$$m_a = \dot{m}_{ai} - \dot{m}_{ao} \tag{24}$$

where $\dot{m}_{ai}$ and $\dot{m}_{ao}$ are the mass flow rates into and out of the intake manifold, respectively. The form of the empirical relationships for these rates are:

$$\dot{m}_{ai} = MAX\ TC(\alpha)\, PRI \tag{25}$$

$$m_{ao} = c_1\ \eta_{vol}\ m_a\ \omega_e \tag{26}$$

where the parameter MAX is the maximum flow rate corresponding to a fully open throttle valve. The function *TC* is the normalized throttle characteristic, a nonlinear function of the throttle angle a. The function *PRZ* is the normalized pressure influence function which is a nonlinear function of the pressure ratio $PR = P_m/P_{atm}$, where P_{atm} is atmospheric pressure. Using the ideal gas law, the manifold pressure, $P_{,,}$ is calculated by

$$P_m = \frac{R\ T_m}{M_{air} V_m} m_a \tag{27}$$

where M_{air} is the molecular weight of air.

The rotational dynamics of the engine is given by:

$$J_e^*\ \dot{\omega}_e = T_{net}(\omega_e, P_m) - T_{load} \tag{28}$$

where T_{net} is the net engine torque defined as the difference between the combustion torque and the torque due to friction and other losses. It is empirically known to be a nonlinear function of the engine speed and the manifold pressure. T_{load} is the effective load torque on the engine. Under the assumptions stated above the vehicle velocity and the engine speed are related by the relation:

$$v = h\, R_g^*\, \omega_e \tag{29}$$

where h the effective tire radius and R_g^* is a variable that depends on the vehicle transmission gear ratio. Consequently the term J_e^* is an effective engine inertia which includes the engine, torque converter, driveshaft, tire and vehicle inertias. Its functional form is therefore:

$$J_e^* = J_e + J_{t,g} + R_g^{*2}\,(J_{wf} + J_{wr} + A\ 4\ h^2) \tag{30}$$

where J_e is the engine and torque converter inertia, $J_{t,g}$ is the transmission inertia in gear g, J_{wf} and J_{wr} are the combined inertias of both front and rear wheels, respectively, and M is the vehicle mass. Included in the expression for the load torque are all the longitudinal dynamics terms (i.e. drag, rolling resistance).

$$T_{load} = R_g\,(T_{bf}\ \cdot\ _I\ -\ T_{br} + C_a\, R_g^{*2}\, h^3\, \omega_e^2 + h\, F_{r,total}) \tag{31}$$

where T_{bf} and T_{br} are the front and rear brake torques, respectively, C_a is a "drag coefficient" (see section 2.1.3), and $F_{r,total}$ is the total rolling resistance.

The final state is the combined brake torque, T_b. Since the brake model is linear and the time constant for the front and rear brake torques is assumed to be same, the two states can be lumped together. The combined dynamics are given by:

$$\tau_{b,v}\, T_b\ +\ T_b\ =\ T_{b,cmd} \equiv K_b\, P_b \tag{32}$$

where and $\tau_{b,v}$ is the brake system time constant, and $K_b = K_{bf} + K_{br}$ is the total brake torque constant of proportionality (see section 2.1)

2.3. Four State Vehicle Model

In order to more accurately model the vehicle dynamics, as compared to the model discussed in section 2.2, we developed a four state vehicle model. In this

development we relax assumption (4) of the previous section. This allows for the inclusion of tire dynamics. These dynamics are particularly important during low velocities and/or high accelerations.

The first state, the mass flow rate of into the intake manifold, remains unaffected by the relaxed assumption. The state equation and auxiliary equations are therefore given by the equations

$$m_a = m_{ai} - m_{ao} \tag{33}$$

$$\dot{m}_{ai} = MAX\ TC(\alpha)\, PRI \tag{34}$$

$$\dot{m}_{ao} = c_1\ \eta_{vol}\ m_a\ \omega_e \tag{35}$$

The rotational dynamics for the engine is given by :

$$J_e'\ \dot{\omega}_e = T_{net}\ (\omega_e\ , P_m) - T_{load} \tag{36}$$

where T_{net} is the net engine torque, a nonlinear function of engine speed and pressure in the manifold obtained from the steady state engine maps. J_e' is the effective inertia of the engine. The load torque T_{load} is given by:

$$T_{load} = R_g^*(T_{br} + hF_{tr}) \tag{37}$$

where R_g^* is the effective gear ratio from the wheel to the engine and h is the effective tire radius. The tractive force F_t is modelled by the following relation:

$$F_t = K_t\, sat(i/0.15) \tag{38}$$

where K_t is the longitudinal tire stiffness and the slip i is given by

$$i = 1 - v/(R_g^*\ h\ \omega_e) \tag{39}$$

The longitudinal equation for the vehicle is given by :

$$M\dot{v} = F_t - C_a v^2 - F_f \tag{40}$$

where c_a is the drag coefficient, F_f is the force due to rolling resistance, and it4 is the effective mass of the vehicle.

The remaining state, the brake torque, remains unchanged by the relaxed

assumption.

$$\tau_{b,v}\, T_b \;+\; T_b \;=\; T_{b,c} \equiv K_b\, P_b \tag{41}$$

2.4. Model Validation

The four state model was partially validated by putting in the same throttle angle to the simulated plant and the actual plant and comparing the velocities of both. Two tests were performed : 1) Constant speed test and 2) Gentle Maneuver test. The respective plots are shown below. It can be seen that the model closely approximates the real plant.

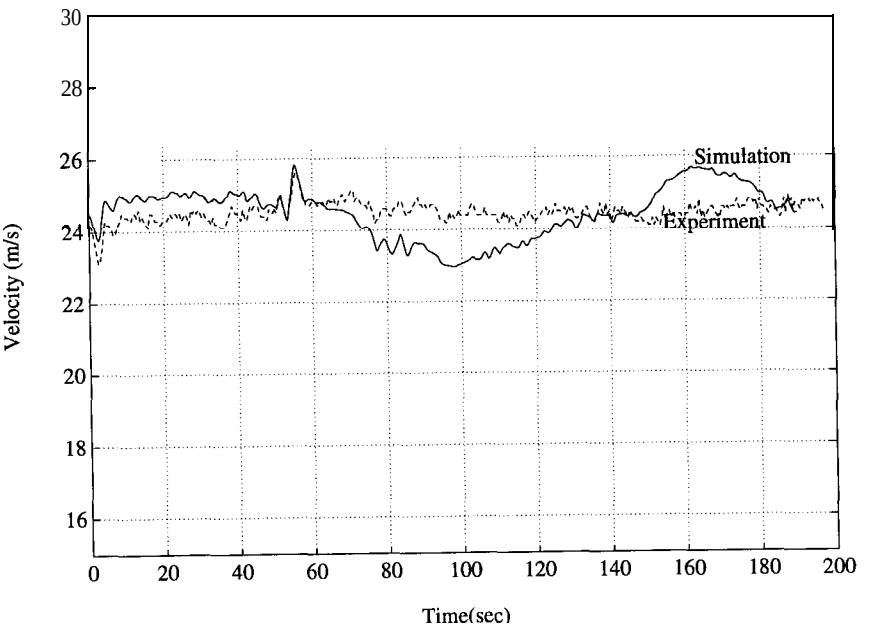

Figure 7: Constant Speed Validation Test

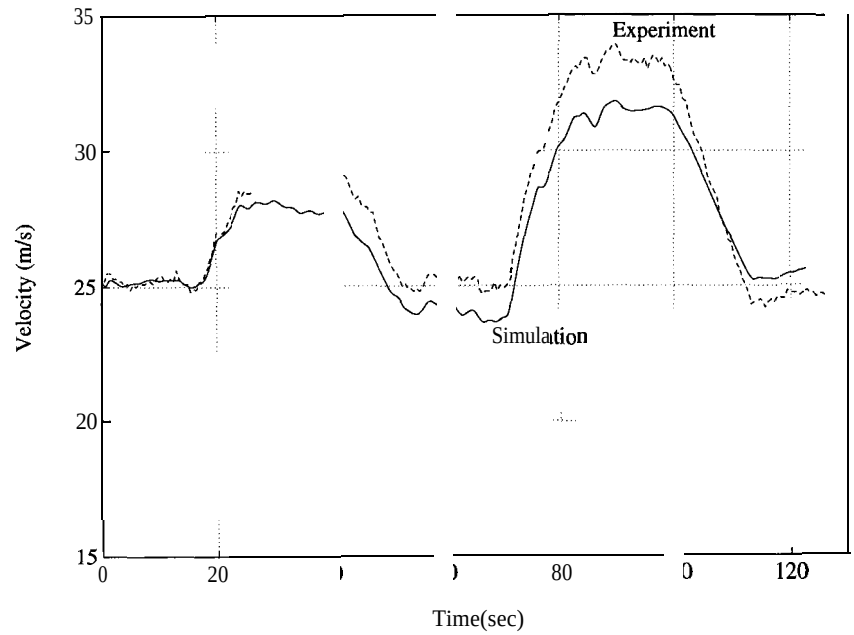

Figure 8: Gentle Maneuver Validation Test

Chapter 3
Platoon Control Algorithms for IVHS

This section presents longitudinal control laws for IVHS based on the three state simplified vehicle model described in sections 2.2. Using spacing and headway as our inter-vehicle criteria, we have investigated several nonlinear control techniques. In section 3.1 we employ the techniques of sliding controls and I/O Linearization to develop spacing controllers. We conclude with a sliding controller for constant-headway IVHS.

3.1. Three State Longitudinal Controller Design

Consider a platoon of N vehicles traveling on a straight lane of highway. Let the i^{th} car behind the lead vehicle be denoted as the i^{th} car in the platoon. Let x_l, v_l, a_l denote the position, velocity and acceleration respectively of the lead car. Let x_i, v_i, a_i be the position, velocity, and acceleration respectively of the i^{th} *car*. Let Δ_i be the distance the i^{th} car wants to keep from the $i-1^{st}$ car. The spacing error for

the i^{th} vehicle ε_i is given by (see Figure 9):

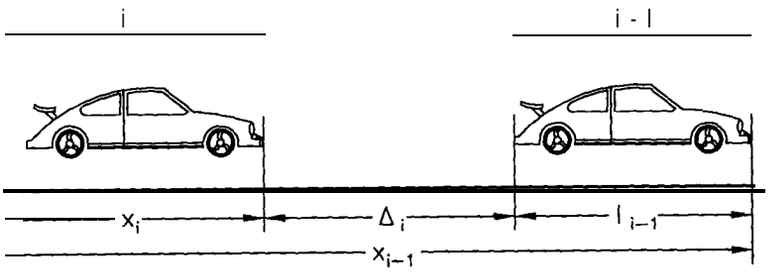

Figure 9: Schematic of the longitudinal platoon control task

$$\varepsilon_i = \Delta_i^d(t) - \Delta_i \tag{42}$$

$$\Delta_i = x_{i-1} - x_i - l_{i-1} \tag{43}$$

It is assumed that the lead vehicle was traveling at a constant speed $v_l(0\_)$ before making a maneuver. It is also assumed that it reaches a constant speed $v_l(t_f)$ after a finite time t_f. Let $w_l(t) = v_l(t) - v_l(0\_)$.

The following are the control objectives:

(1) Each vehicle closed loop system should be asymptotically stable.

(2) The effect of the lead vehicle's velocity change on the spacing error of the first vehicle should be as small as possible. It is also required that all the spacing errors, resulting from any lead vehicle maneuver, go to zero asymptotically.

(3) Furthermore, to avoid amplification of spacing errors, it is required that the spacing errors decrease down the platoon.

It is assumed that the following measurements are accessible :

For simplicity we will consider the vehicles to be point masses. Consequently, the distance l_{i-1} is zero and will be omitted from the following discussions.

(1) Engine speed.

(2) Pressure in the manifold.

(3) Range and closing rate to the preceding vehicle.

(4) Preceding vehicle's acceleration.

(5) Lead vehicle's velocity and acceleration.

3.1.1. Sliding Controller Design

One design methodology to achieve the above objectives was to use *Sliding Controls.* This is a robust design technique that compensates for nonlinearities in the vehicle plant. In particular we use a multiple surface technique [6,7,8]. Following the control formulation by Hedrick, McMahon, Narendran, and Swaroop [7] with lead vehicle feedforward information, we define:

$$S_{1i} = \dot{\varepsilon}_i + q_1 \varepsilon_i + q_2 \int_{t_o} \varepsilon_i \, dt + q_3 (v_i - v_{lead}) \tag{44}$$

Differentiating (assuming Δ_i^d = constant), we define

$$\dot{S}_{1i} \equiv -\lambda_1 S_{1i} \tag{45}$$

Following the multiple surface approach, we define a synthetic control,

$$\dot{\omega}_{e,d} = \frac{a_{i-1} - \mathbf{41} \dot{\varepsilon}_i - q_2 \varepsilon_i - \lambda_1 S_{1i} + q_3 a_{lead}}{(1 + q_3) R_g^* h} \tag{46}$$

Substituting into equation 27 yields the desired net torque:

$$T_{net,d} = J_e^* \dot{\omega}_{e,d} + R_g^* (T_{br} + T_{bf}) + R_g^* h F_{f,total} + C_a R_g^{*3} h^3 \omega_e^2 \tag{47}$$

Using a table look-up procedure with data from steady state engine maps, the

desired mass of air in the intake manifold, $m_{a,d}$ can be calculated. We now define the second surface as:

$$S_{2i} \equiv m_a - m_{a,d} \tag{48}$$

Following the sliding control formulation and using equation 23 we have:

$$S_{2i} = m_{ai} - m_{ao} - \dot{m}_{a,d} \equiv -\lambda_2 S_{2i} \tag{49}$$

Substituting for $\dot{m}_{ai}$ we can solve for the desired throttle characteristic,

$$TC_{i,d}(\alpha) = (\dot{m}_{ao} + \dot{m}_{a,d} - \lambda_2 S_{2i}) / (MAX\ PRI) \tag{50}$$

The desired throttle control angle is determined by simply inverting the throttle characteristic. A negative desired throttle angle is used as the criterion for when to use the brakes for control.

For the case of longitudinal control using brake pressure, we use equations 28 and 3 1 to solve for a desired brake torque.

$$T_{b,d} = \frac{T_{net} - h\ R_g^*(C_a R_g^{*2} h^2 \omega_e^2 + F_{f,total}) - J_e^* \dot{\omega}_{e,d}}{R_g^*} \tag{51}$$

Next, we define

$$S_{3i} \equiv T_{b,i} - T_{b,d} \tag{52}$$

Setting $\dot{S}_{3i} = -\lambda_{3i} S_{3i}$ we can solve for

$$T_{b,c} = \tau_b\ (\dot{T}_{b,d} - \lambda_{3i}\ S_{3i}) + T_{b,i} \tag{53}$$

The commanded brake pressure can be calculated by simply dividing by the constant, K_b (see equation 32).

3.1.2. I/O Linearization Controller Design

In order to accomplish the above mentioned objectives an approach utilizing Input-Output Linearization was developed. I/O Linearization also compensates for the non-linearities in the plant and hence, it is well suited for this problem.

The desired output in the I/O Linearization formulation is the position of the i^{th} vehicle.

$$y_1 = x_i \tag{54}$$

Differentiating,

$$\dot{y}_1 = \dot{x}_i \tag{55}$$

$$\ddot{y}_1 = \ddot{x}_i = R_g^* h(T_{net} - RT_{br} - \phi)/J_e^* \tag{56}$$

where

$$\phi = R_g^*(hF_f + c_a R_g^{*2} h^3 \omega_e^2) \tag{57}$$

The desired net engine torque T_{nd} from the engine is chosen to be

$$T_{nd} = R_g^* T_{br} + \phi + Ju_i/R_g^* h \tag{58}$$

If we need to brake, the desired brake torque T_{bd} is given by

$$T_{bd} = (T_{net} - \phi)/R_g^* - Ju_i/R_g^{*2} \quad h \tag{59}$$

With these choices of torques, the plant dynamics now becomes :

$$\ddot{x}_i = u_i \tag{60}$$

where u_i, a synthetic input, is chosen to accomplish the desired objectives. The desired mass of air in the manifold (m_{ad}) is interpolated from the steady state engine maps knowing m_a and ω_e. Synthetic outputs m_a and T_{br} are defined and it is desired that m_a and T_{br} track m_{ad} and T_{bd} respectively so that the desired net torque to place the vehicle at the correct position is obtained.

$$y_2 = m_a \tag{61}$$

$$\dot{y}_2 = \dot{m}_a = MAXTC(\alpha)\, PRI(m_a) - \dot{m}_{ao} \tag{62}$$

The desired throttle angle (α_d)is chosen such that

$$TC(\alpha_d) = (\dot{m}_{ao} - \lambda_2 (m_a - m_{ad}) + \dot{m}_{ad})/(MAX\ PRI(m_a)) \tag{63}$$

where $\dot{m}_{ad}$ is obtained from numerical differencing.

The constant λ_2 is chosen to be less than the bandwidth of the throttle actuator. If $\alpha_d < \alpha_0$, the braking should occur. In this case,

$$y_3 = T_b \tag{64}$$

$$\dot{y}_3 = \dot{T}_b = (T_{bc} - T_b)/\tau_b \tag{65}$$

Choose T_{bc} such that

$$T_{bc} = T_b + \tau_b (\dot{T}_{bd} - \lambda_3 (T_b - T_{bd})) \tag{66}$$

As in the previous case, T_{bd} is obtained by numerical differencing. λ_3 is chosen to be less than the bandwidth of the brake actuator.

Consider the most general form of the control law given by :

$$\begin{aligned} u_i = {} & -k_p \varepsilon_i - k_v \dot{\varepsilon}_i + k_a \ddot{x}_{i-1} + k_1 (v_{i-1}(t) - v_{i-1}(0\_)) \\ & - c_p (x_i - x_l + \sigma) - c_v (v_i - v_l) + k_l a_l \qquad i = 2,3,4,..... \end{aligned} \tag{67}$$

$$\begin{aligned} u_1 = {} & -(k_p + c_p)\varepsilon_1 - (k_v + c_v)\dot{\varepsilon}_1 + (k_a + k_l) a_l \\ & - k_1 (v_l(t) - v_l(0\_)) \end{aligned} \tag{68}$$

where the constants $k_p, k_,, k_a, k_l, k_1, c_p, c_v$ are to be determined. The transfer functions relating the spacing error of the first vehicle (ε_i) to the lead vehicle velocity deviation (w_l) and the spacing error of the i^{th} vehicle to that of the $i-1^{st}$ vehicle are as follows:

$$\hat{g}(s) = \frac{\hat{\varepsilon}_1}{\hat{w}_l}(s) = \frac{(k_a + k_l - 1)s + k_1}{s^2 + (k, + c_v)s + (k_p + c_p)} \tag{69}$$

$$\hat{h}(s) = \frac{\hat{\varepsilon}_i}{\hat{\varepsilon}_{i-1}}(s) = \frac{k_a s^2 + (k, + k_1)s + k_p}{s^2 + (k, + c_v)s + (k_p + c_p)} \tag{70}$$

Reiterating the control objectives, (1) For closed loop stability, the characteristic polynomial should be Hurwitz, i.e

$$k_v + c_v > 0 \; ; \; k_p + c_p > 0 \tag{71}$$

(2) The effect of lead vehicle's velocity change on the spacing error of the first vehicle should be as small as possible at all frequencies. Since it is required that the spacing error of all vehicles go to zero asymptotically, $k_1 = 0$. With this choice of k_1, the two transfer functions are given by

$$\hat{g}(s) = \frac{(k_a + k_l - 1)s}{s^2 + (k_v + c_v)s + (k_p + c_p)} \tag{72}$$

$$\hat{h}(s) = \frac{k_a s^2 + k_v s + k_p}{s^2 + (k_v + c_v)s + (k_p + c_p)} \tag{73}$$

(3) A necessary condition for avoiding spacing error amplification is that $|\hat{h}(j\omega)| < 1$ at all frequencies. At this point, it is apparent that the reduction in $|\hat{h}(j\omega)|$ at low frequencies is aided by lead vehicle's position feedback, at middle frequencies by lead vehicle's velocity feedback and at high frequencies by lead vehicle's acceleration feedback. Having no lead vehicle's position feedback is equivalent to setting c_p to zero. The two transfer functions are :

$$\hat{g}(s) = \frac{(k_a + k_l - 1)s}{s^2 + (k_v + c_v)s + k_p} \tag{74}$$

$$\hat{h}(s) = \frac{k_a s^2 + k_v s + k_p}{s^2 + (k_v + c_v)s + k_p} \tag{75}$$

For $|\hat{h}(j\omega)| < 1$ the following condition has to be satisfied:

$$c_v > \sqrt{k_v^2 + 2k_p(1 - k_a)} - k_v \tag{76}$$

By setting $k_a + k_l = 1$, $\hat{g}$ (s) is made equal to zero. It is also necessary to ensure that the spacing error dynamics is much slower than the dynamics of the

synthetic output. In order to achieve the performance objectives, the above constraints have to be satisfied. The resulting control laws are:

$$u_i = -k_p\,\varepsilon_i - k_v\,\dot{\varepsilon}_i + k_a\,\ddot{x}_{i-1} - c_v\,(v_i - v_l) + k_l\,a_l \qquad i=2,3,4,..... \quad (77)$$

$$u_1 = -(k_p + c_p)\varepsilon_1 - (k_v + c_v)\dot{\varepsilon}_1 + (k_a + k_l)a_l - k_1(v_1(t) - v_1(0\_)) \quad (78)$$

The frequency response plot of $\hat{h}(j\omega)$ is shown in Figure 10.

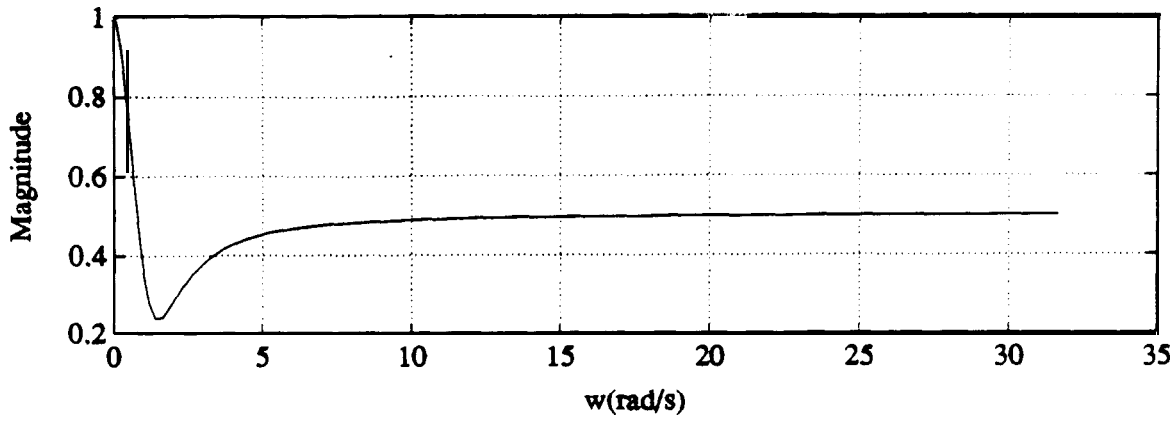

Figure 10a: Magnitude plot for $\hat{h}$ (jo).

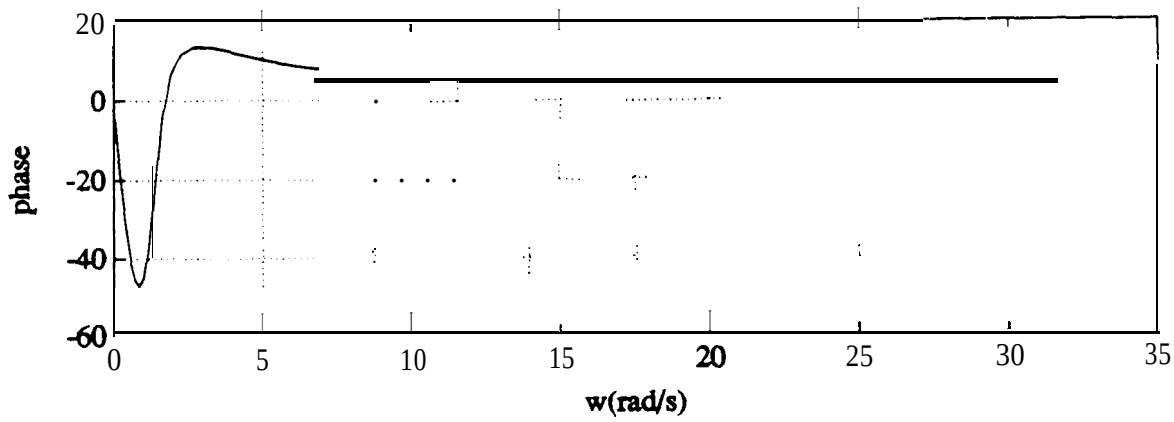

Figure 10b: Phase plot for $\hat{h}$ (jo).

3.1.3. Controller Equivalence Conditions

Since the method of *Sliding Controls* is a special case of I/O Linearization there exist equivalence relations between the control laws presented in sections 3.1.1 and 3.1.2. The synthetic control in the sliding control formulation was given by the equation 46:

$$\dot{\omega}_{e,d} = \frac{a_{i-1} - q_1 \dot{\varepsilon}_i - q_2 \varepsilon_i - \lambda_1 S_{1i} + q_3 a_{lead}}{(1 + q_3) h R_g^*} \tag{79}$$

The corresponding control input for the I/O Linearization technique was given by the equation:

$$\begin{aligned} u_i &= a_{i,des} = \omega_e h R_g^* \\ &= -k_p \varepsilon_i - k_v \dot{\varepsilon}_i + k_a \ddot{x}_{i-1} - c_v (v_i - v_l) + k_l a_l \quad i = 2,3,4,. \end{aligned} \tag{80}$$

By substituting for S_{1i} with $q_2 = 0$ (no integral action) the control input (equation 79) reduces to:

$$\begin{aligned} \omega_{e,des} = {} & \frac{1}{R_g^* h} \left\{ \frac{1}{1 + q_3} a_{i-1} + \frac{q_3}{1 + q_3} a_l - \frac{\lambda_1 + \lambda_1}{1 + q_3} \dot{\varepsilon}_i \right\} \\ & + \frac{1}{R_g^* h} \left\{ - \frac{\lambda_1 \lambda_1}{1 + q_3} \varepsilon_1 - \frac{\lambda_1 q_3}{1 + q_3} (v_i - v_l) \right\} \end{aligned} \tag{81}$$

comparing coefficients for $\omega_{e,des}$ we obtain the following five equivalence and two constraint equations, respectively:

$$k_a = \frac{1}{1 + q_3} \tag{82}$$

$$k_l = \frac{q_3}{1 + q_3} \tag{83}$$

$$k_v = \frac{\lambda_1 + \lambda_1}{1 + q_3} \tag{84}$$

$$k_p = \frac{\lambda_1 \lambda_1}{1 + q_3} \tag{85}$$

$$c_v = \frac{\lambda_1 q_3}{1 + q_3} \tag{86}$$

$$k_a + k_l = 1 \tag{87}$$

$$\lambda_1 k_a + c_v = \lambda_1 \tag{88}$$

3.2. Headway Longitudinal Controller Design

In this section, a control law for maintaining constant headway is developed using a two-surface sliding scheme. The control law is based on the three state model. The three states are:

(1) Mass of air in the manifold (m_a).

(2) Engine speed (w_e).

(3) Brake Torque (T_{br}).

The following are the equations upon which the controller is based.

$$\dot{m}_a = MAX\ TC(\alpha)\, PRI(m_a) - \dot{m}_{ao} \tag{89a}$$

$$\dot{\omega}_e = (T_{net}\ (\omega_e, m_a) - T_l)/J_e^* \tag{89b}$$

$$J_e^* = J_e + J_{t,g} + R_g^{*2}\,(Mh^2 + 2 \cdot J_w) \tag{89c}$$

$$T_b = (T_{bc} - T_b)/\tau_b \tag{89d}$$

$$T_{load} = R(T_b + hF_f + C_a R^2 h^3 \omega_e^2) \tag{89e}$$

Consider a platoon of N vehicles traveling on a straight lane of highway. Let the i^{th} car behind the lead vehicle be denoted as the i^{th} car in the platoon. Let x_l, v_l, a_l, denote the position, velocity and acceleration of the lead vehicle respectively and let x_i, v_i, a_i respectively denote the position, velocity and acceleration of the i^{th} vehicle. Let h_w be the headway time to be maintained and L_i be the safe separation. Then, define δ_i as

$$\delta_i = x_{i-1} - Xi - L_i \tag{90}$$

$$\varepsilon_i = \delta_i - h_w \dot{x}_i \tag{91}$$

Define the first surface S_1 as

$$S_1 = \varepsilon_i \tag{92}$$

$$\dot{S}_1 = \dot{\delta}_i - h_w \ddot{x}_i = \dot{\delta}_i - h_w R_g^* h(T_{net} - R_g^* T_b - \phi_l)/J_e^* = -\lambda_1 S_1 \quad (93)$$

whence, the desired net engine torque T_{nd} is given by

$$T_{nd} = R_g^* T_b + \phi_l + J_e u_1 / R_g^* h \tag{94}$$

where

$$u_1 = (\dot{\delta}_i + \lambda_1 S_1)/h_w \tag{95}$$

Once T_{nd} is calculated, desired mass of air in the manifold m_{ad} is found by interpolation from the steady state engine maps.

$$S_2 = m_a - m_{ad} \tag{96}$$

$$\dot{S}_2 = \dot{m}_a - \dot{m}_{ad} = -\lambda_2 S_2 \tag{97}$$

$$TC(\alpha_d) = (\dot{m}_{ao} + \dot{m}_{ad} - \lambda_2 S_2)/MAX\ PRI(m_a) \tag{98}$$

where $\dot{m}_{ad}$ is obtained by numerical differentiation of m_{ad} and α_d is found from the tables by interpolation knowing *TC*. If $\alpha_d < \alpha_0$, then braking should occur. The desired braking torque T_{bd} is given by

$$T_{bd} = (T_{net} - \phi_l - Ju_1/R_{g*}\ h)/R_g^* \tag{99}$$

Define another surface S_3 as

$$S_3 = T_b - T_{bd} \tag{100}$$

$$S_3 = T_b - T_{bd} = -\lambda_3 S_3 \tag{101}$$

$$T_{bc} = T_b + \tau_b(\dot{T}_{bd} - \lambda_3 S_3) \tag{102}$$

In this controller design it is important to note that:

(1) The spacing errors ε_i are completely independent from one another since $\dot{\varepsilon}_i + \lambda_1 \varepsilon_i = 0$.

(2) For maintaining a spacing of 12 meters at 25 m/s, the headway time required is 0.2 seconds. Typical values of load torque and other relevant parameters are :

$$R_g^* h = 0.1$$
$$J_e^*/R_g^* h = 220.0$$
$$\phi_l = R_g^* h(F_f + C_a v^2) = 0.1(\ 167 + 0.5 \cdot 25^2) = 50.0$$
$$T_{nd} = 50.0 + 220\ (\dot{\delta}_i + \lambda_1 S_1) / h_w \qquad (103)$$

With the spacing control law, the net torque is given by

$$T_{nd} = 50 + 220\ (\ddot{x}_l + \ddot{x}_{i-1} + \varepsilon_i + \dot{\varepsilon}_i + 3(v_i - v_l)) / 2 \qquad (104)$$

For an initial velocity error of 0.1 m/s for a 2-car platoon, the net desired engine torque is around 160 Nm, while only 90Nm is required for the spacing control law. As this error increases, the difference in torque required increases. From the control law, the effort required is inversely proportional to the headway.

Chapter 4
Longitudinal Platoon Control - Simulation Results

4.1. Complex Vehicle Model: Spacing Control

In this section we present simulation results for a four car platoon of 1990 Ford Lincoln Town Cars under closed loop control. The mathematical representations of the vehicles are given by the twelve state model described in section 2.1. Results presented in this section are obtained using the multi-surface sliding controller outlined in section 3.1.1. The maneuver illustrated here is a typical acceleration profile from one constant cruise velocity to another.

Figure 1 la shows that the velocity tracking is very acceptable producing spacing errors of less than 2 cm. As designed the spacing error is not amplified as the vehicle number in the platoon increases.

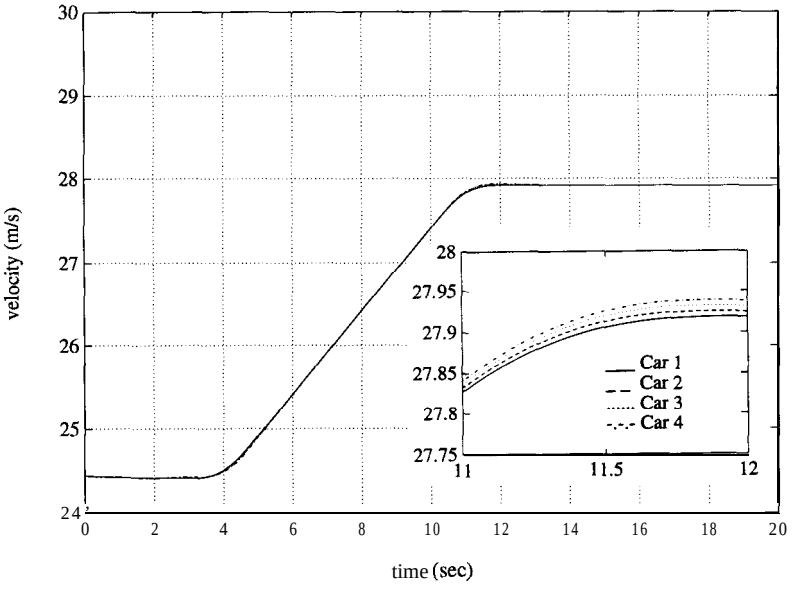

Figure 1 la: Four car platoon simulation results for complex vehicle model: vehicle velocities

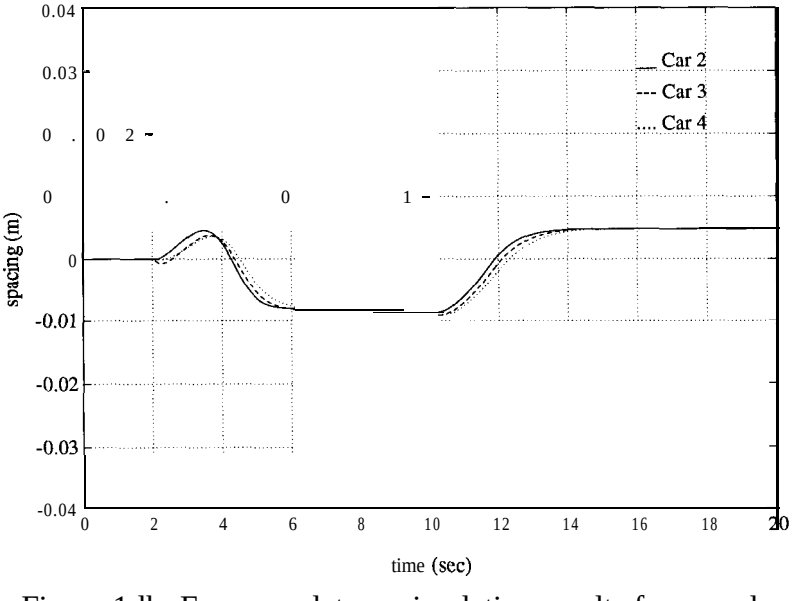

Figure 1 lb: Four car platoon simulation results for complex vehicle model: spacing error

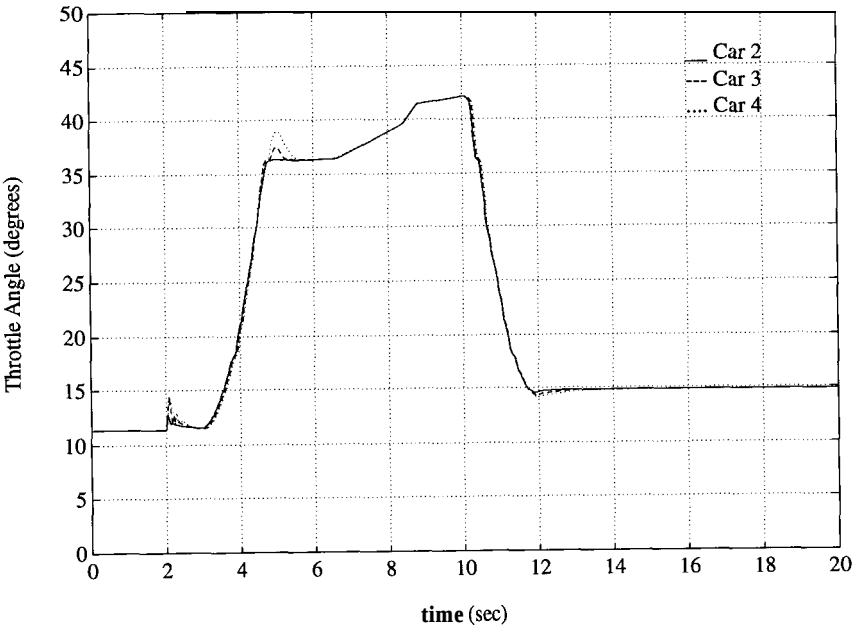

Figure 1 lc: Four car platoon simulation results for complex vehicle model: throtlle control signals

4.2. Four State Vehicle Model: Spacing Control

The simulation results presented in this section are for a ten (10) car platoon (a lead vehicle and nine following vehicles). The lead vehicle velocity profile is a specified function of time. The simulated vehicles are the four-state simplified mathematical representations of the experimental 1990 Ford Lincoln Town cars (see section 2.2.3). All nine trailing vehicles are under closed loop control using the I/O linearization algorithm presented in section 3.1.2. The control update time is 53 milliseconds. Lead vehicle velocity and acceleration information is assumed to be communicated every 53 milliseconds. The gains chosen are k_p = 1, k_v = 0.5, c_v = 1.5, $k_a = k_l$ = 0.5. These were based upon the control design criteria given by equations 71 and 76.

Figures 12a, b, c show results for the typical maneuver described above. Velocity tracking is quite good throughout the entire maneuver. It is important to note that the spacing error between consecutive vehicles decreases as the vehicle number in the platoon increases. The control law has successfully eliminated the problem of spacing error amplification in platoons.

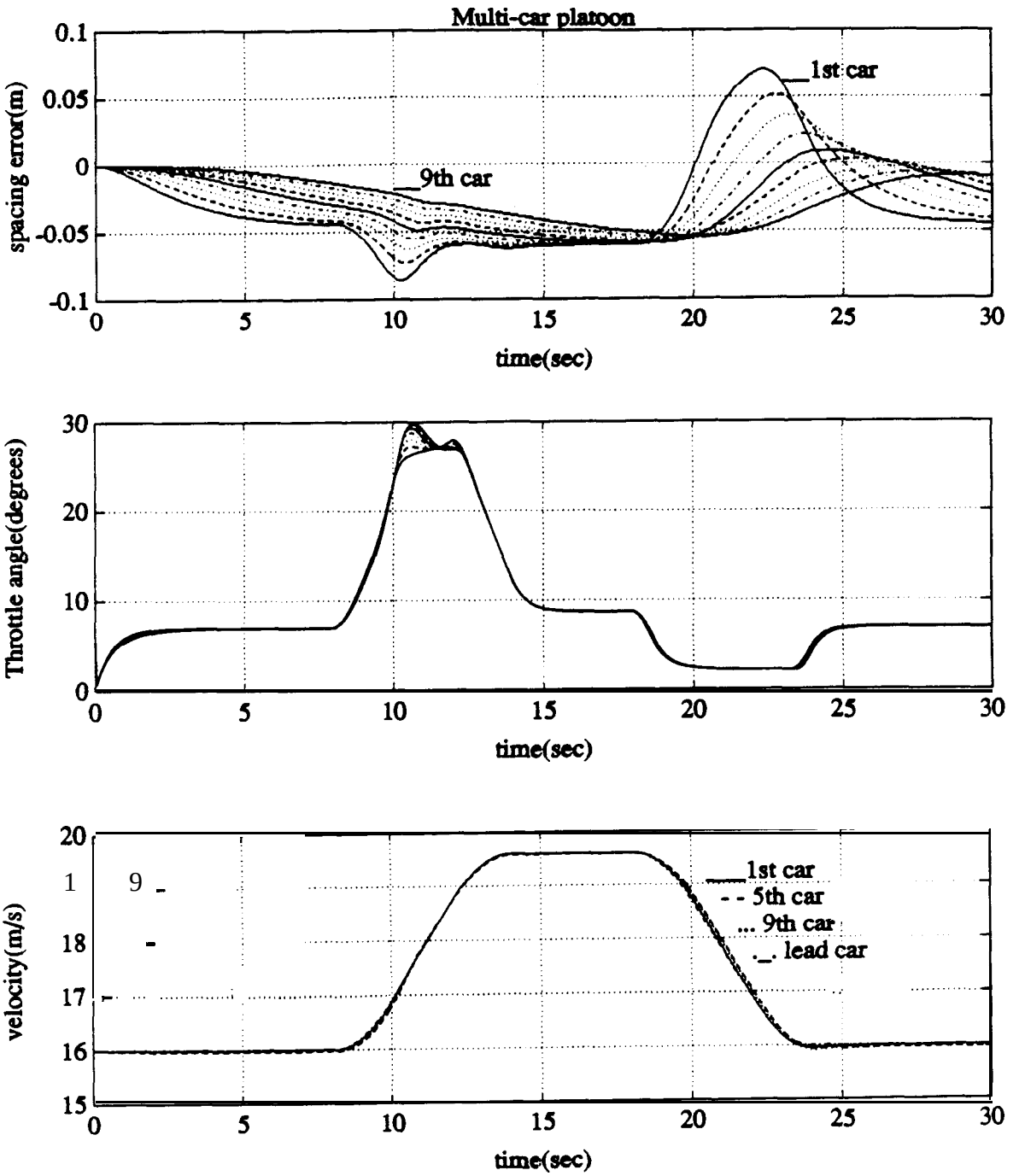

Figure 12: Ten car platoon simulation results for reduced order model

4.3. Three State Vehicle Model: Headway Control

Simulations were performed for a lo-car platoon using the constant headway and constant spacing control laws. In both the cases, the lead car was made to perform the same gentle maneuver. $\lambda_1 = 5.0$, $\lambda_2 = 40.0$ and $\lambda_3 = 2.5$ were chosen for these simulations.

Test 1:

All the cars in the platoon start with zero errors in initial conditions. Simulation results for the platoon under spacing and headway control are shown in Figures 13 & 14, respectively. It can be seen that the net engine torque required is considerably higher in the constant headway control case and consequently, the throttle angles are higher.

Test 2:

Only the first car has an initial spacing error of $0.6m$. Results of simulation are illustrated in Figures 15 & 16 Examining the acceleration plots, the ride quality for the constant headway platoon seems to degrade significantly with increasing vehicle number in the platoon, as compared to the spacing based controller.

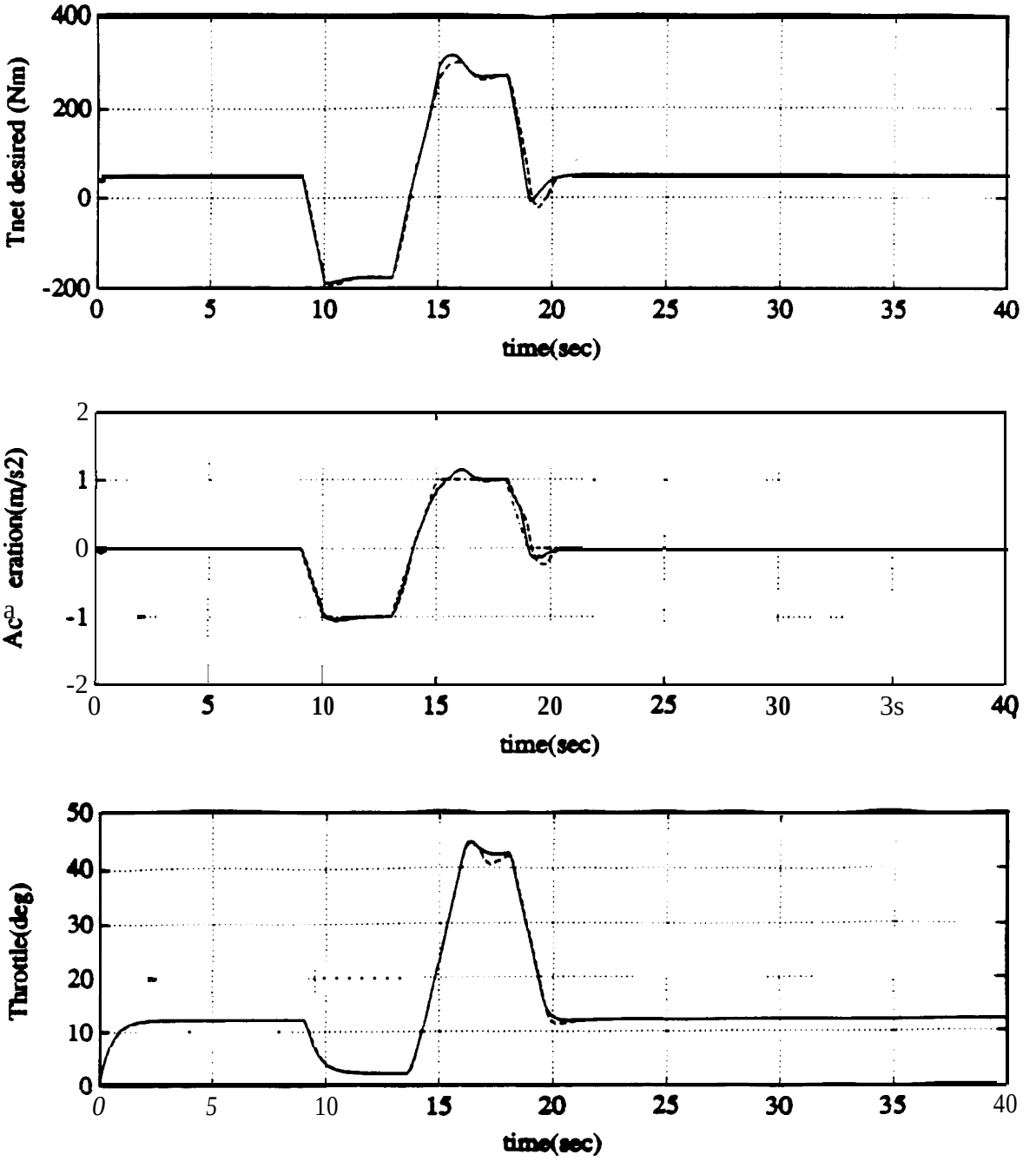

Figure 13: Ten car platoon simulation results using spacing-based controller - Zero initial conditions.

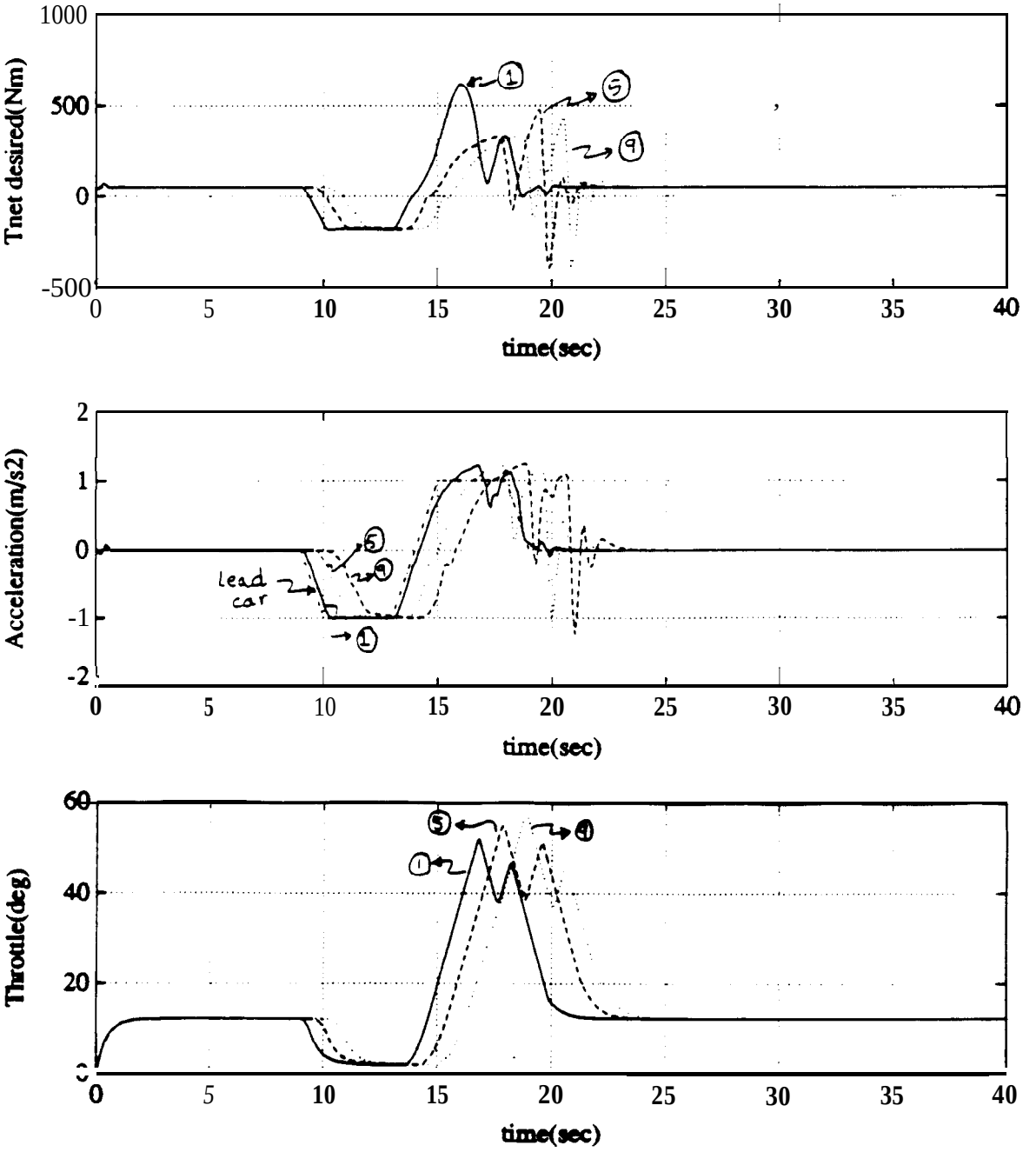

Figure 14: Ten car platoon simulation results using headway-based controller - Zero initial conditions.

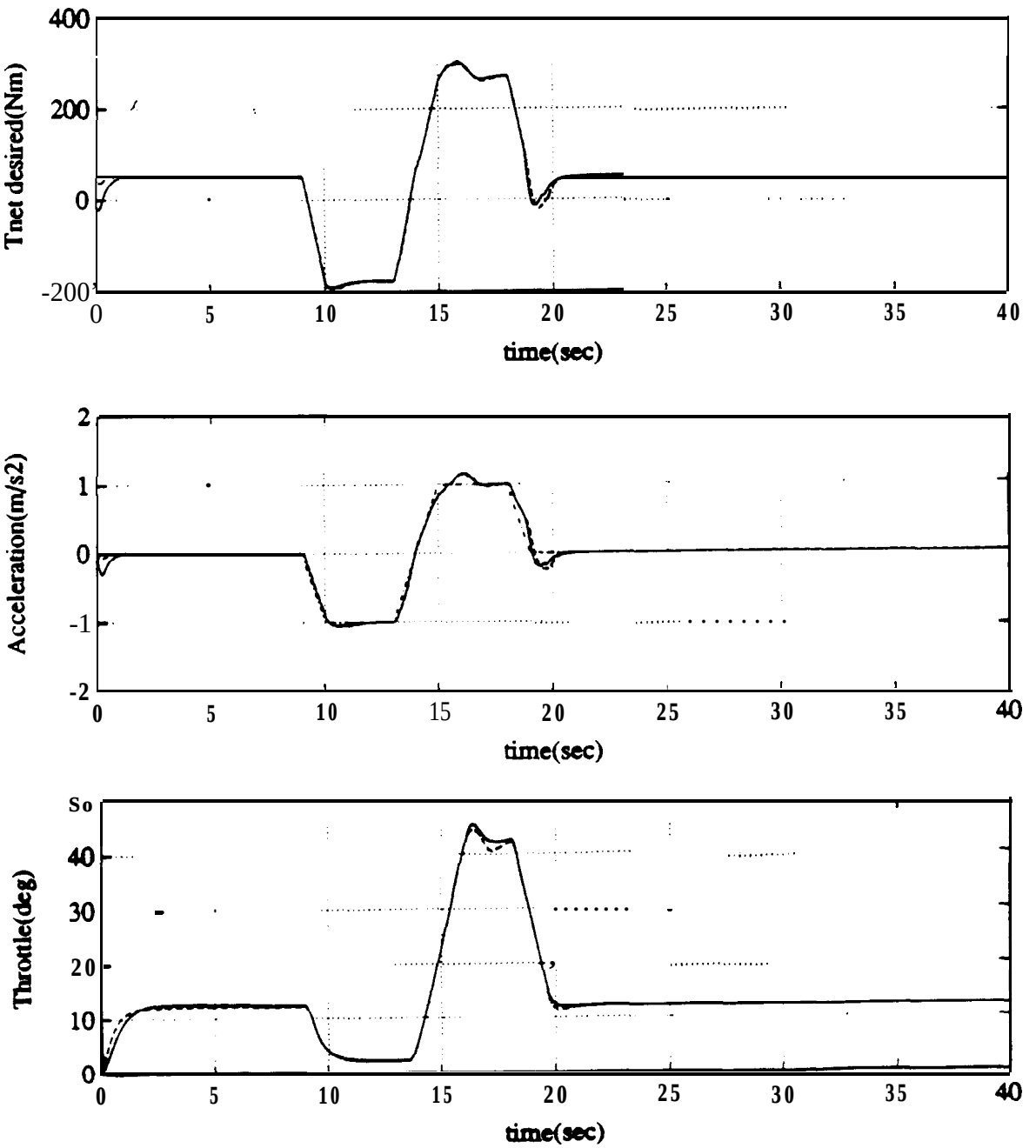

Figure 15: Ten car platoon simulation results using spacing-based controller - Non-zero initial conditions.

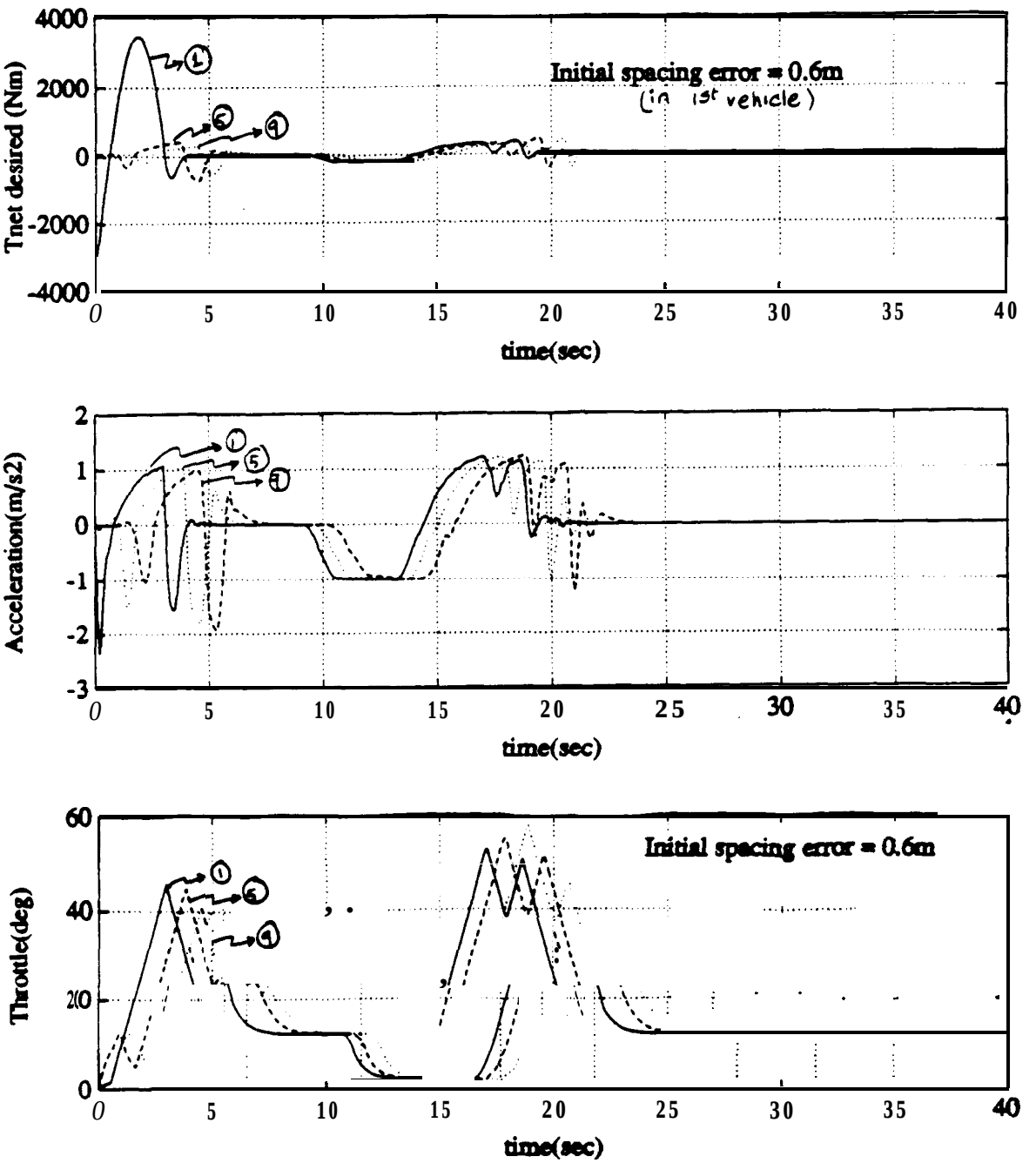

Figure 16: Ten car platoon simulation results using headway-based controller - Non-zero initial conditions.

Chapter 5
Implementation Issues

In the process of developing the vehicle follower control system it was necessary to address several implementation concerns. Among these issues are computer speed and memory, specifications of the data acquisition system, actuator specifications, sensor accuracy and precision, and communication system reliability and speed. This section will only address the issues related to the actuators. The two actuators used in longitudinal control are connected to the throttle and brake system.

5.1. Actuator Specifications

The actuator specification tests were divided into two categories, open loop and closed loop. Open loop tests were used to determine the minimal required throttle saturation rate and the minimal brake actuator bandwidth for acceptable vehicle response. Closed loop tests were used to evaluate the minimal required throttle

actuator bandwidth and the minimal brake actuator saturation rate. All results were determined using a typical V-6 front wheel drive simulation model.

The time responses used to determine the minimal throttle saturation rate were the throttle step response (see Figure 17) and the spacing deviation from the lead vehicle (see Figure 18). Minimum rise time of the throttle response and minimum spacing deviation were the selected performance criteria. The required throttle rate was selected to be $\geq$ 400 degrees/sec. There was no significant improvement in either response beyond this point.

The time response of the distance between two successive vehicles was used for the throttle bandwidth studies. (see Figure 19). Using minimum deviation from a desired spacing distance as our performance measure, the minimal required throttle actuator bandwidth was selected to be 10Hz. There was no marked improvement beyond the selected 10Hz bandwidth.

A step input in commanded brake pressure was chosen to evaluate the brake actuator bandwidth and saturation rate requirements. The responses of interest for these performance tests were those of the vehicle velocity and vehicle acceleration. A 5Hz bandwidth was determined to be the minimal required bandwidth (see Figure 20 & 21). A value of (Maximum Torque)/0.1sec was determined to be acceptable (see Figures 22 & 23). In all cases, there was no significant improvement in the system responses beyond the selected specifications.

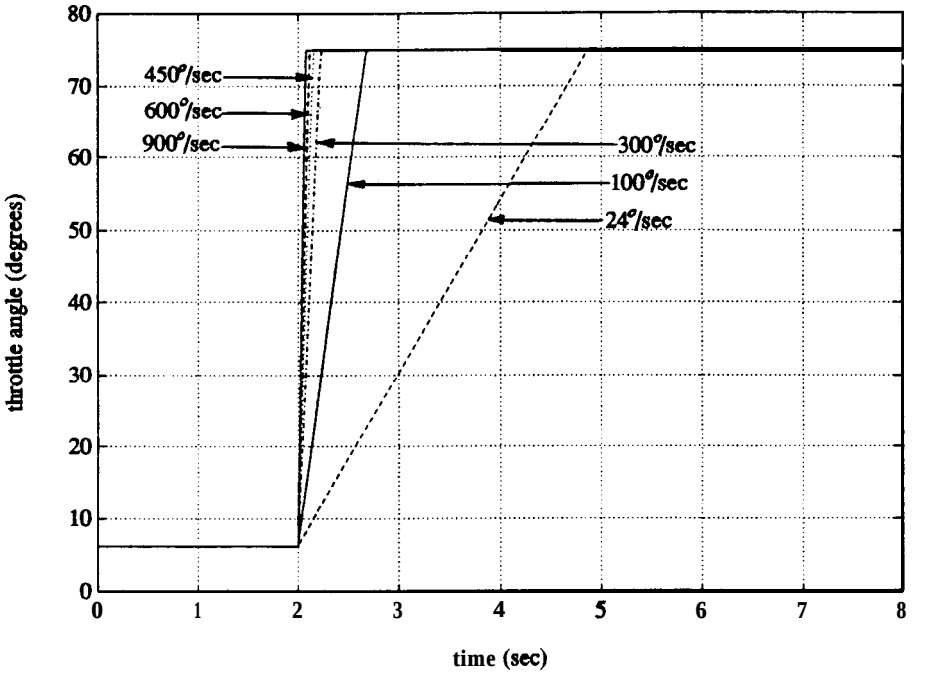

Figure 17: Open loop throttle step response tests for various saturation rates (Randwidth 100Hz)

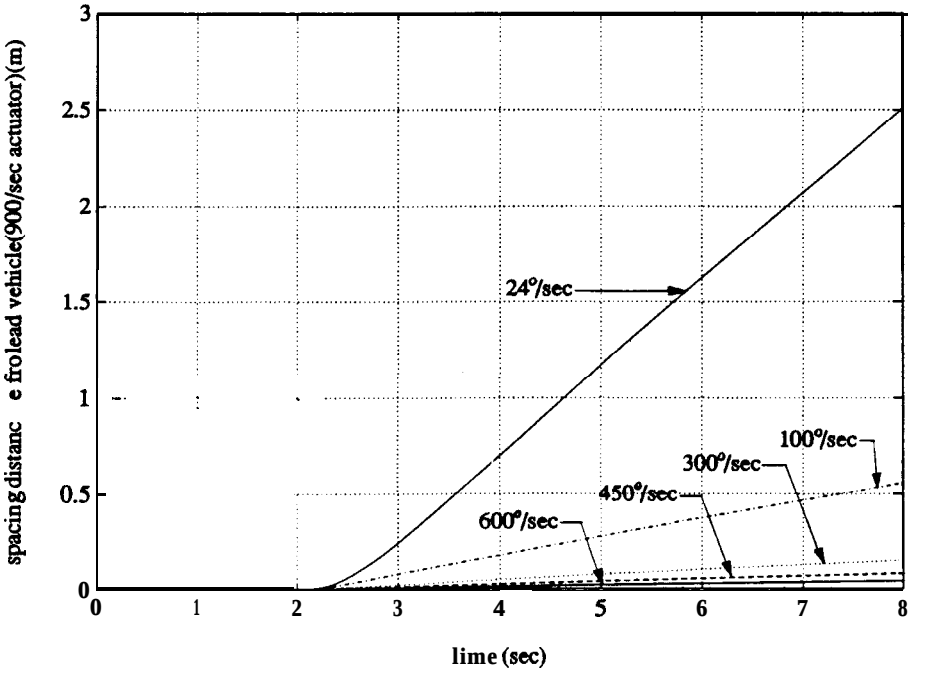

Figure 18: Spacing deviation from lead vehicle for various throttle saturation rates (Bandwidth 100hz)

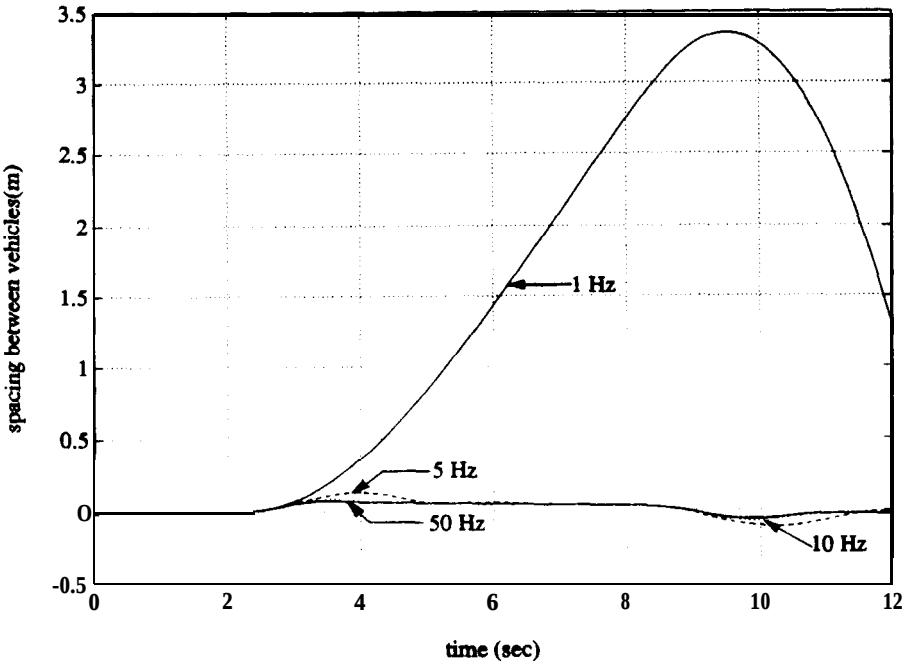

Figure 19: Spacing distance between successive vehicles for various throttle actuator bandwidths (Saturation Rate $900^o/sec$)

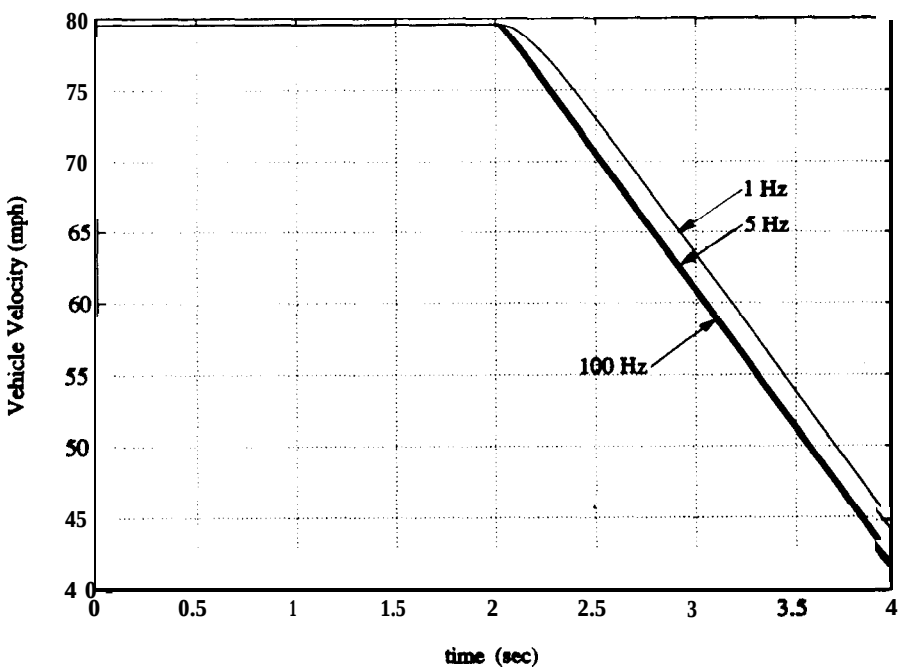

Figure 20: Vehicle velocity during full braking for various brake actuator bandwidths

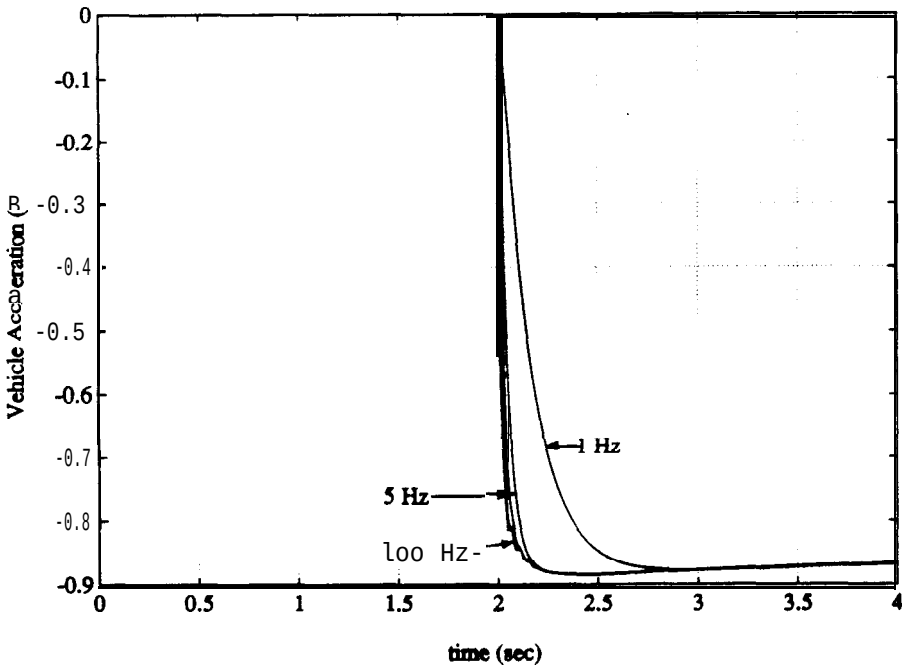

Figure 2 1: Vehicle acceleration during full braking for various brake actuator bandwidths

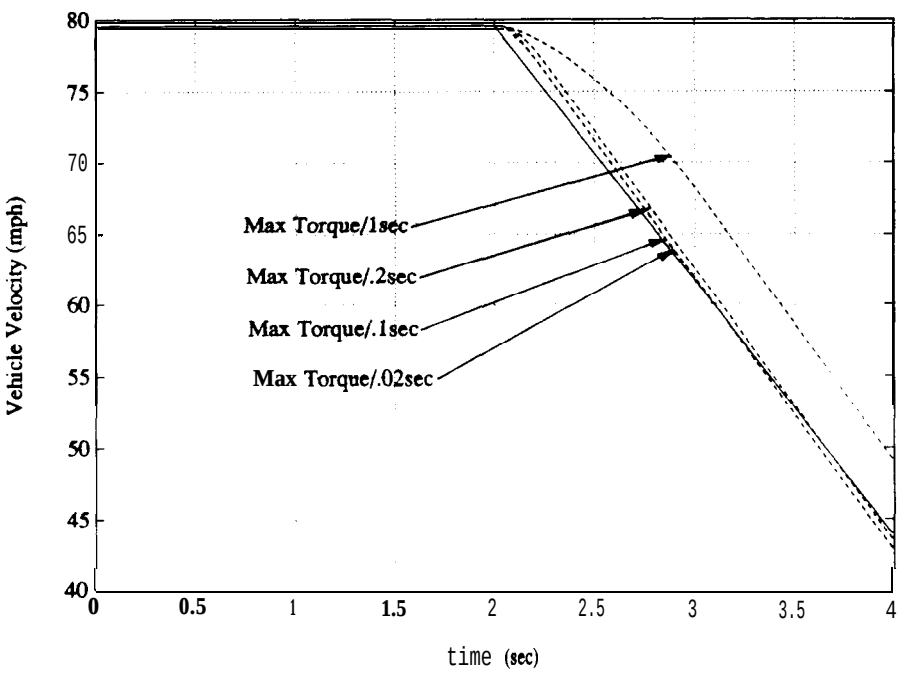

Figure 22: Vehicle velocity during a platoon maneuver for various brake actuator saturation rates (Bandwidth 5Hz)

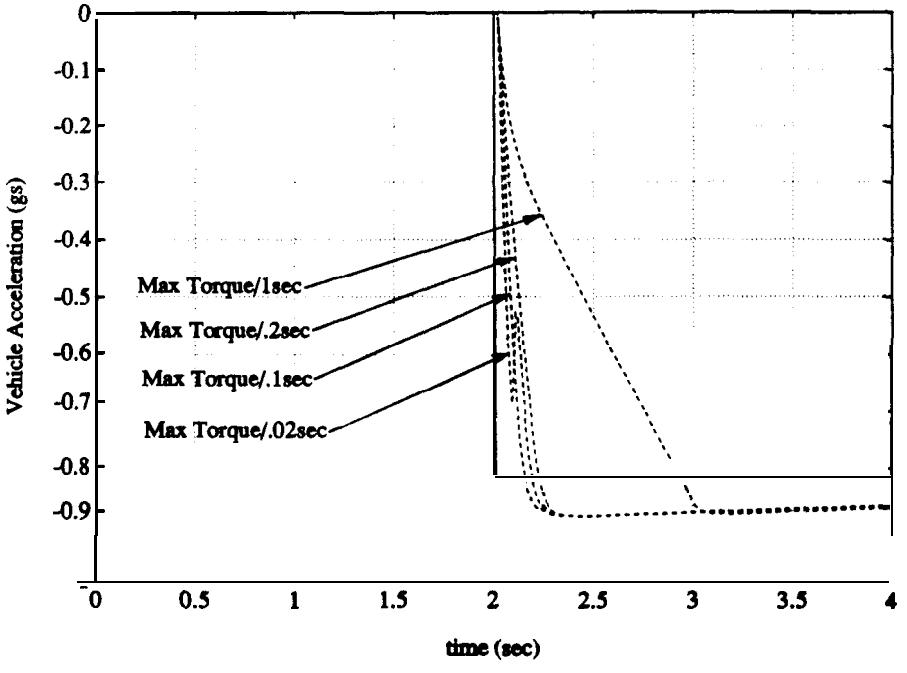

Figure 23: Vehicle acceleration during a platoon maneuver for various brake actuator saturation rates (Bandwidth 5Hz)

5.2. Brake Actuator Control and Testing

A pulse-width-modulation scheme was chosen to control the pneumatic brake actuator. This method was selected since the easiest computer signal to produce is a binary one and the most efficient way to modulate power is with amplifiers that are full on or full off.

The period chosen for the PWM signal was 100ms. This 10Hz signal was high enough in frequency that the brake line pressure did not have time to respond to the rapid on-off changes, consequently reflecting the average power level over many cycles. A PWM signal frequency higher than 10Hz would have been so fast that for small duty cycles the pneumatic actuator could not respond in time. The minimal

duration for a high pulse to be effective was approximately 15-20ms.

A hardware solution to the problem of creating the necessary PWM signal was chosen. A schematic of the brake actuator control circuit is shown below. The circuit accepts an analog voltage between OV and 5V and produces the corresponding duty cycle. However, the 0% duty cycle and 100% duty cycle correspond to 1V and 4V, respectively. The PWM frequency is specified by the choice of resistors and capacitors. This was a first generation design intended for preliminary testing. Features to account for temperature variations and changes in component values over time were not considered at this time.

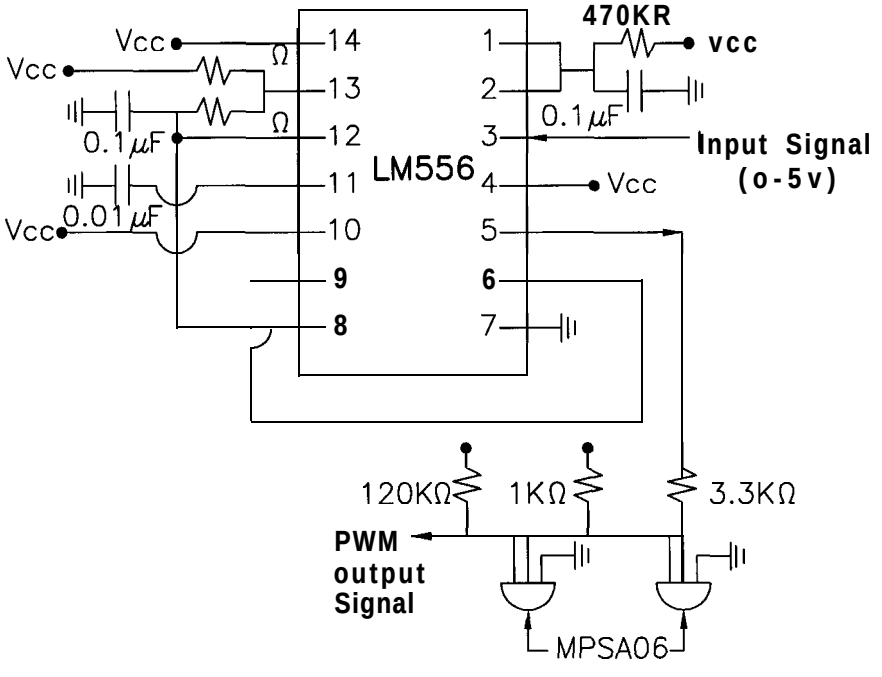

Figure 24: Schematic of brake system interface circuit.

The input-output relationship between voltage and brake line pressure was found to be nonlinear. A curve fit equation to the experimental data for input voltage (V) vs brake line pressure (P_b) is given by (see Figure 25):

$$V = 1.2214\ P_b^2 + 2.9176\ P_b + 0.7677 \tag{105}$$

where V is given in units of volts and P_b is given in units of psig * 10^{-3}.

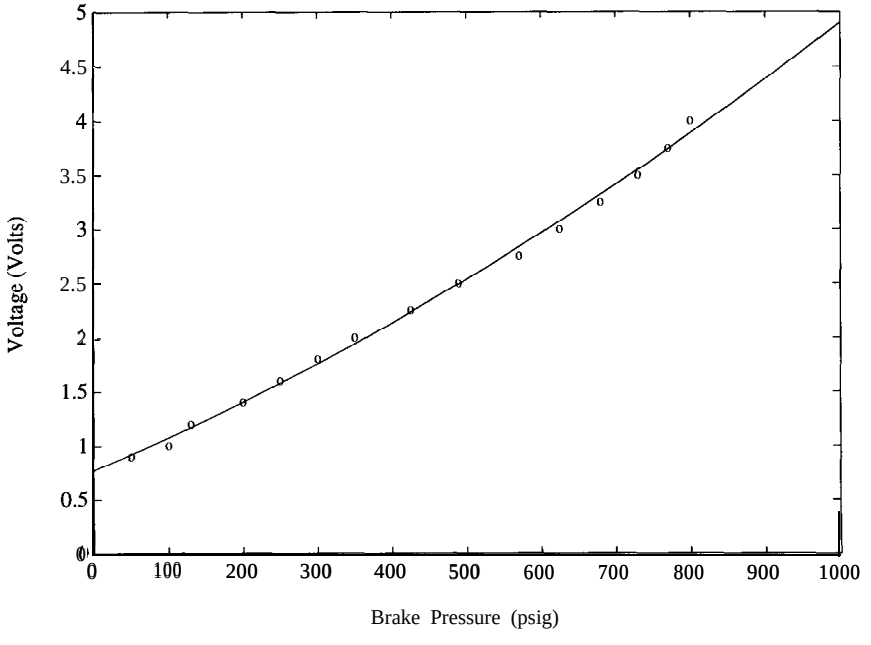

Figure 25: Brake circuit input voltage vs. brake pressure

The brake system, consisting of the vehicle brake system and pneumatic actuator, can be modelled with a nonlinear block, a normalizing block, and a first order lag block (see Figure 26). The input to the system is a commanded brake pressure. The output is the vehicle brake pressure. The time constant associated with the brake system is $\tau_{b,t} = 0.25 sec$. The brake torque is obtained by simply multiplying

the brake pressure by K_b, the brake torque proportionality constant.

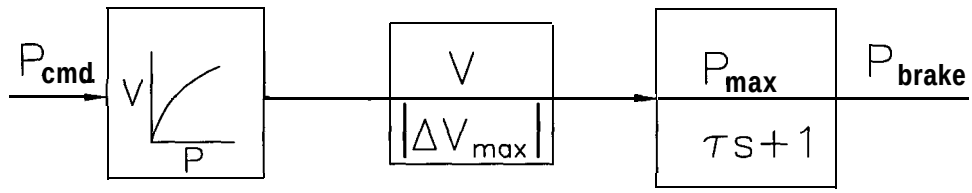

Figure 26: Block diagram of brake system model

Using the above model for the actual brake system it can be shown that the current system is too slow to meet the tracking requirements for the vehicle following problem. Also, experimental testing indicates that the brake system is subject to a load dependent vacuum boost. This additional variable posses an added difficulty in accurate control of the brake pressure. Due to the inadequecy of the system it will be replaced by a hydraulic brake system.

Chapter 6
Experimental Platoon Development

6.1. Integrated Platoon Control System (IPCS)

The Integrated Platoon Control System (IPCS) is described in detail by K.S. Chang, et al.[3]. The IPCS consists of the following components (see Figure 27):

(1) 80386 based personal computers

(2) radar distance sensors manufactured by VORAD Safety Systems, Inc.

(3) digital radio transceivers and communication interface boards

(4) data acquisition boards

(5) Sensors: speed, acceleration, throttle angle, brake pressure, engine speed, intake manifold pressure and temperature

(6) throttle and brake actuators

(7) data storage systems

The VORAD radar antennas are mounted at the centers of the front grilles of the three Ford Lincoln Town Cars. They are used to measure the distance and closing rate between a vehicle and the vehicle preceding it.

The communication is performed using a radio link through spread-spectrum digital transceivers. Each of the transceivers is controlled by a communication interface board installed in the on-board computer. Radio communication is accomplished via two cellular phone type coaxial antennas. The communication format is based upon a token passing scheme. The lead vehicle transmits its time clock, vehicle speed and acceleration to the second vehicle. The latter receives this data and transmits it along with its velocity and acceleration to the next vehicle. This process it repeated throughout the platoon. Each trailing vehicle uses its information to calculate the throttle and brake command signals.

The IPCS uses the modified sliding control algorithm described in section 2. In the two car platoon, the controller in the following car uses eleven measurements (see items 2 & 5 above) in addition to the measurements transmitted from the preceding vehicle. The actuation signals calculated by the algorithm command the throttle and brake actuators via the data acquisition board. During these tests only throttle control was used.

All the measurements are input to the data acquisition board to be processed for the control inputs. The nine signals are sampled every 53 ms using the channel scanning method. In synchronization with sampling, the control loop is iterated every 53 ms.

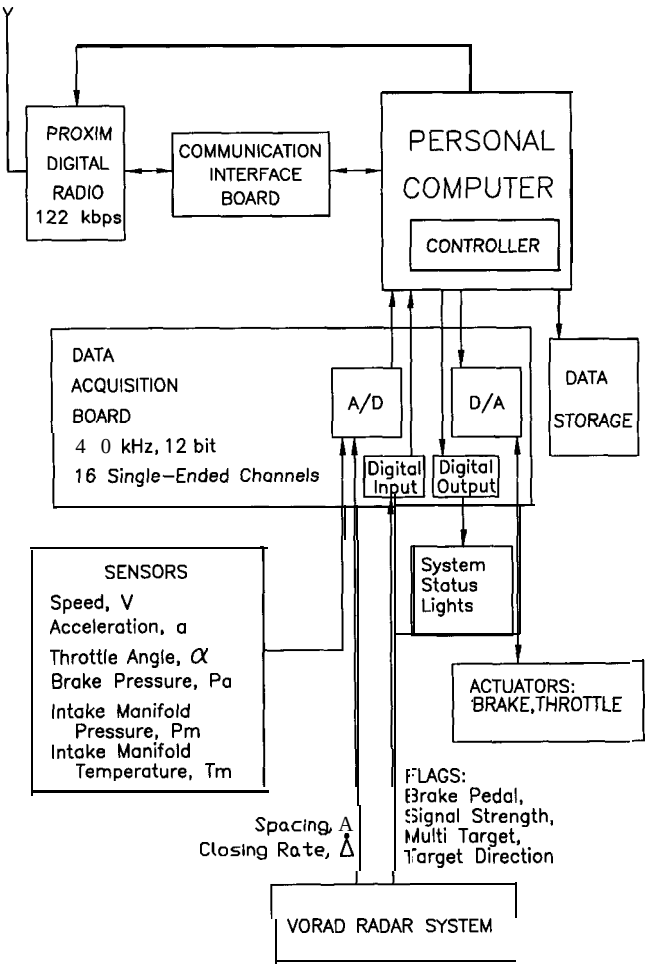

Figure 27: Overall System Configuration

6.2. The Operating Environment

The real-time operating system VRTX-PC was chosen as the host environment for the IPCS . Within the IPCS the following tasks were performed: control law calculation, communication, data acquisition, data transfer, data storage, error handling, and user interfacing. Although VRTX-PC allows tasks to run under different priorities and with various scheduling policies (multitasking) these features were

not utilized at that time. All tasks were given equal priority and accomplished sequentially in 53ms. Only the screen display features of VRTX were used.

6.3. IPCS Experimental Results

6.3.1. Two Car Testing

For this first phase of testing only two cars were used. The lead car was driven manually while the following vehicle was under automatic longitudinal control. The test driver in the following vehicle was responsible for lateral control. In the two car platoon, the lead vehicle is always in transmitting mode while the following vehicle is always in receiving mode.

The tests were conducted on an eight mile HOV lane on I-15 in San Diego. Both vehicles were accelerated under manual control to a desired steady state speed with an approximate separation distance of 30 ft (9.14 meters). At this stage both vehicles were switched to their respective automatic control modes. The following vehicle is under complete longitudinal control.

The two different tests performed were as follows:

(1) Test Mode 1: Lead vehicle maintained constant speed (55 mph) (Figures 28a,b,c).

(2) Test 2: Lead vehicle executed a specified acceleration/deceleration profile (maximum acceleration = 0.05g; maximum deceleration = 0. lg) (Figures 29a,b,c).

In Test 1 the desired separation between the cars was set to be 30 ft (9.14 meters). The control system compensated for any initial condition mismatches and reached a steady state after approximately 5 seconds of test time. Range deviations

were generally kept within 0.5 meters of the desired value during the entire maneuver.

Test 2 was conducted with similar initial conditions. In general, the tracking was good, with range deviations of less than one meter during the maneuver. The velocity of the following car was very close to the desired velocity profile of the leading vehicle.

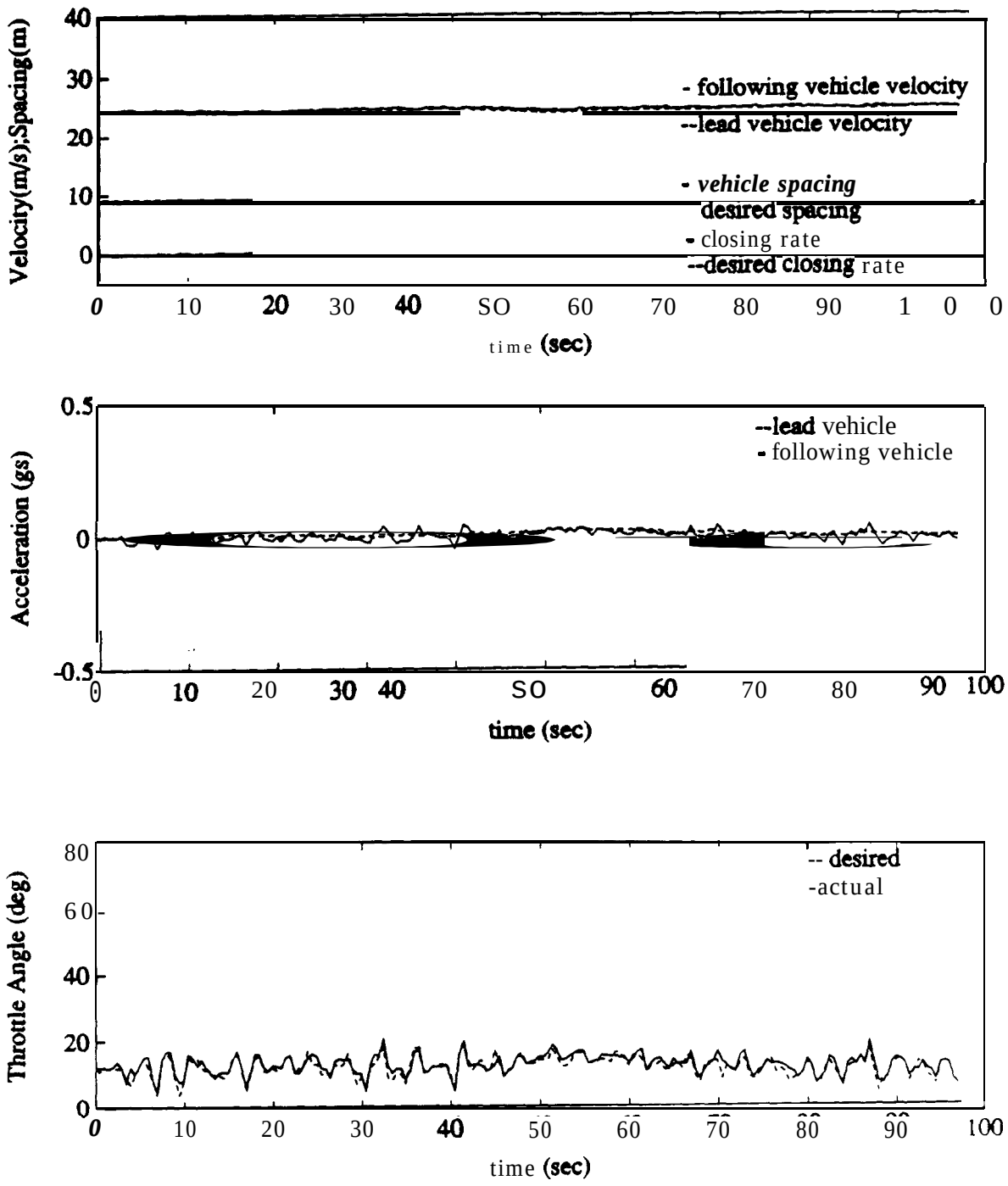

Figure 28: Two car platoon results for Test 1.

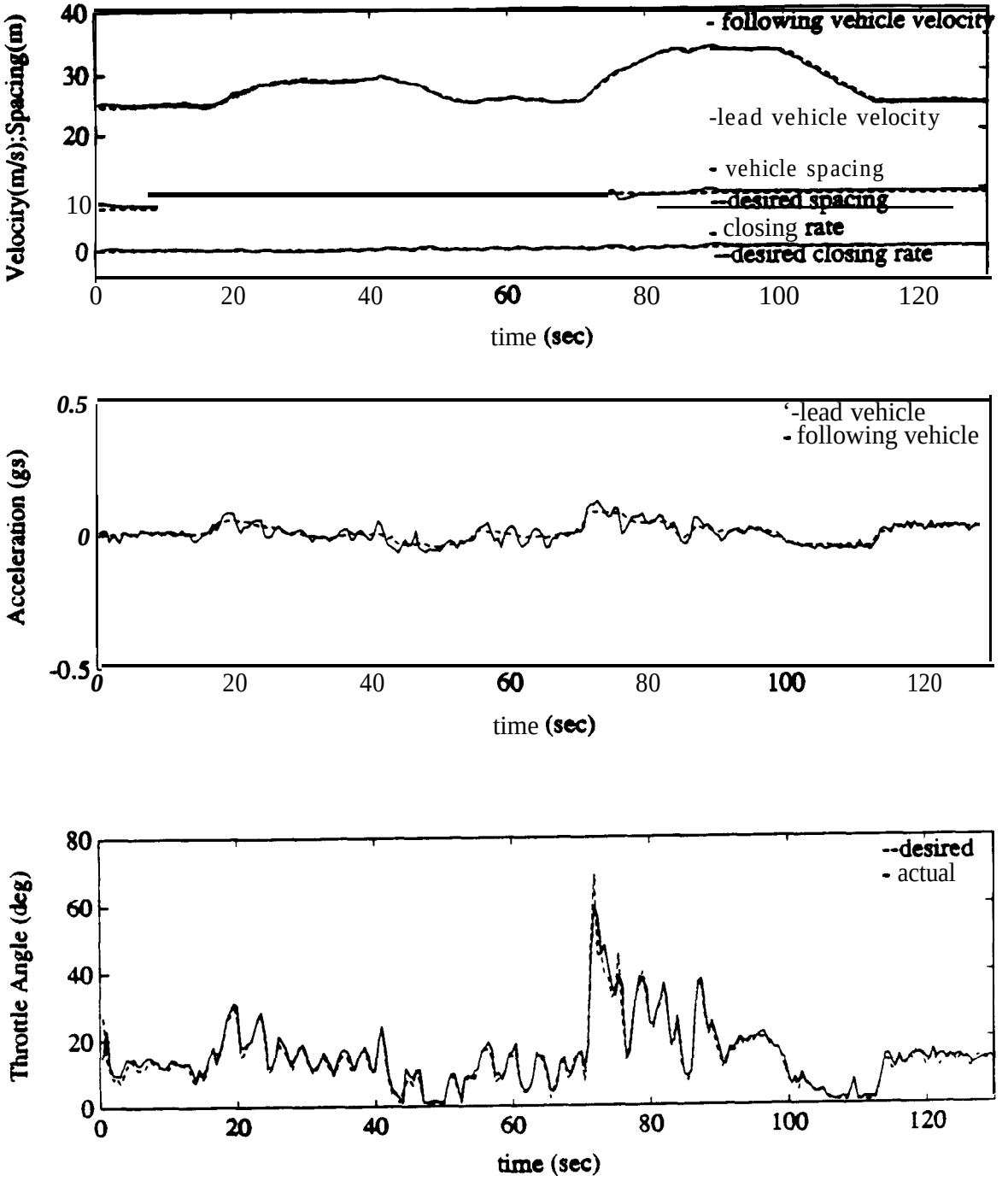

Figure 29: Two car results for Test 2.

6.3.2. Four Car Platoon Testing

During the second phase of testing four vehicles were used. The lead vehicle was again manually driven while the following vehicles were under automatic longitudinal control. All drivers were responsible for lateral control of their respective vehicles. In four-car platoon testing, each vehicle alternates between transmission and reception modes.

The four-car platoon tests were conducted on the HOV lane on I-15 in San Diego. As in the two-car case, all vehicles were accelerated under manual control to a specified velocity, at which point each switched to automatic mode. Desired separation distances ranged between 30 and 70 feet. Results for a constant and variable lead vehicle velocity profile are shown in figures 31 and 32, respectively. Range deviation for the constant velocity tests as well as the variable velocity tests were typically less than 1 meter.

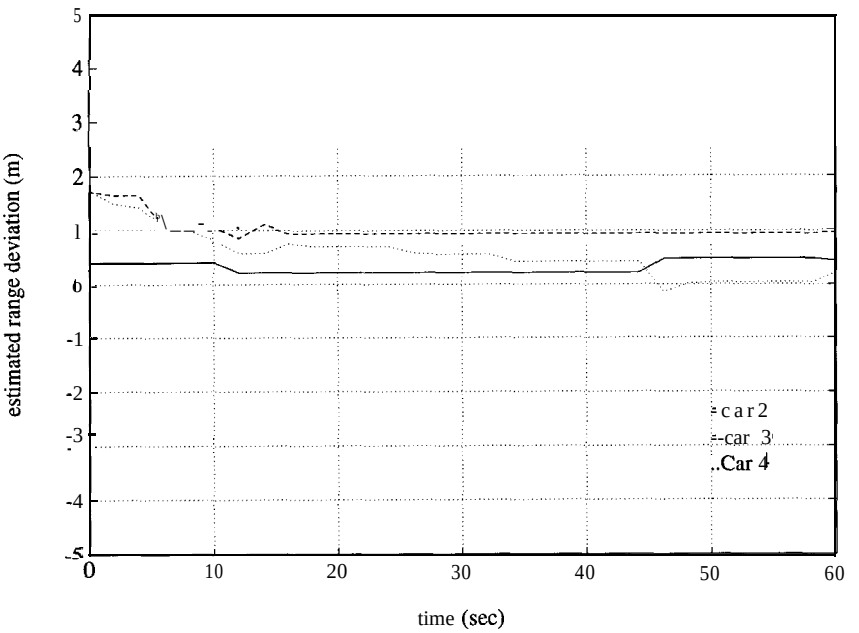

Figure 30a: Four car platoon estimated range deviation: Constant velocity profile.

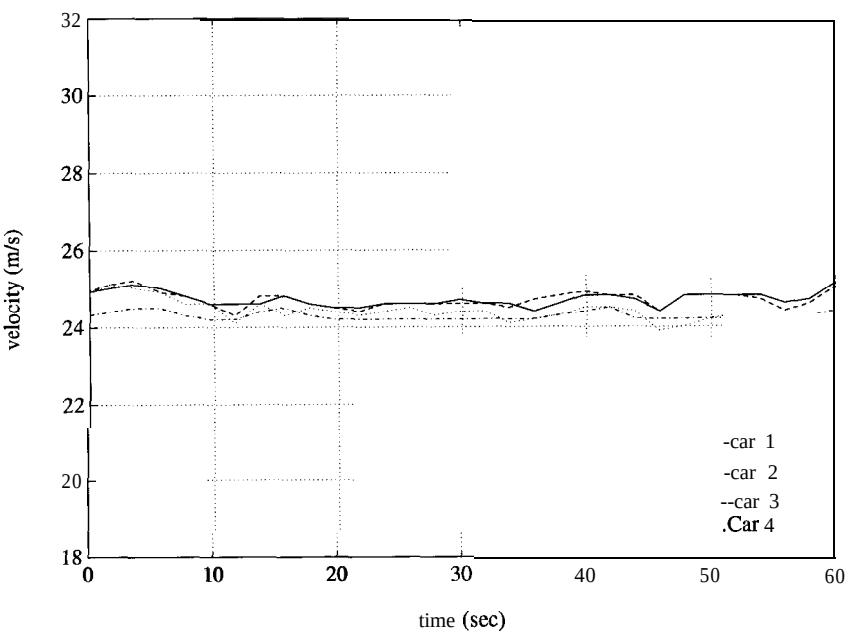

Figure 30b: Four car platoon velocities: Constant velocity profile.

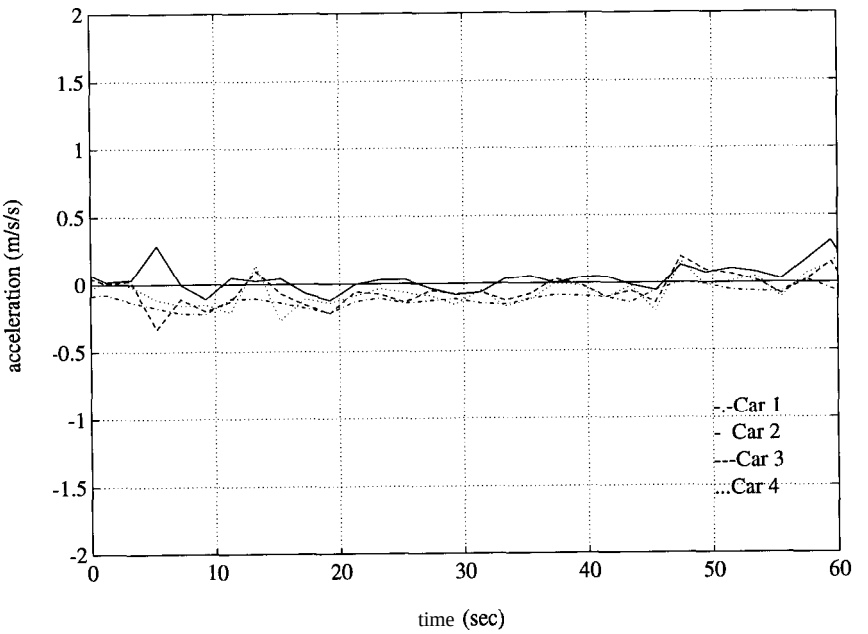

Figure 30c: Four car platoon accelerations: Constant velocity profile.

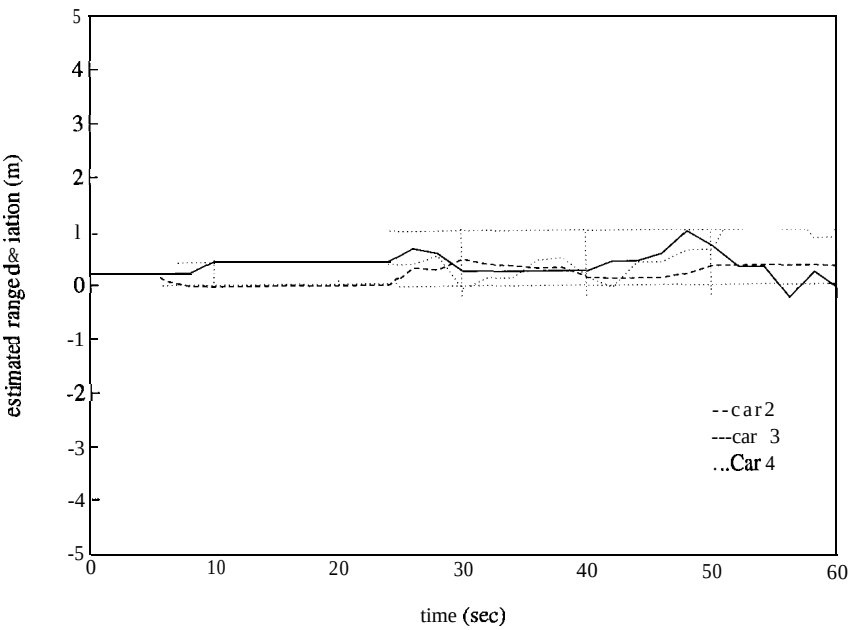

Figure 3 la: Four car platoon estimated range deviation: Variable velocity profile.

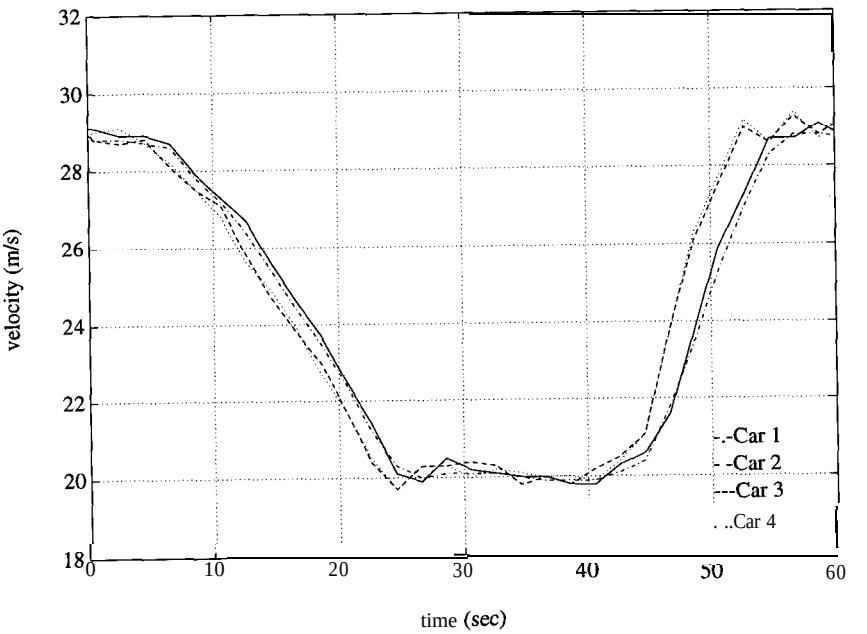

Figure 3 lb: Four car platoon velocities: Variable velocity profile.

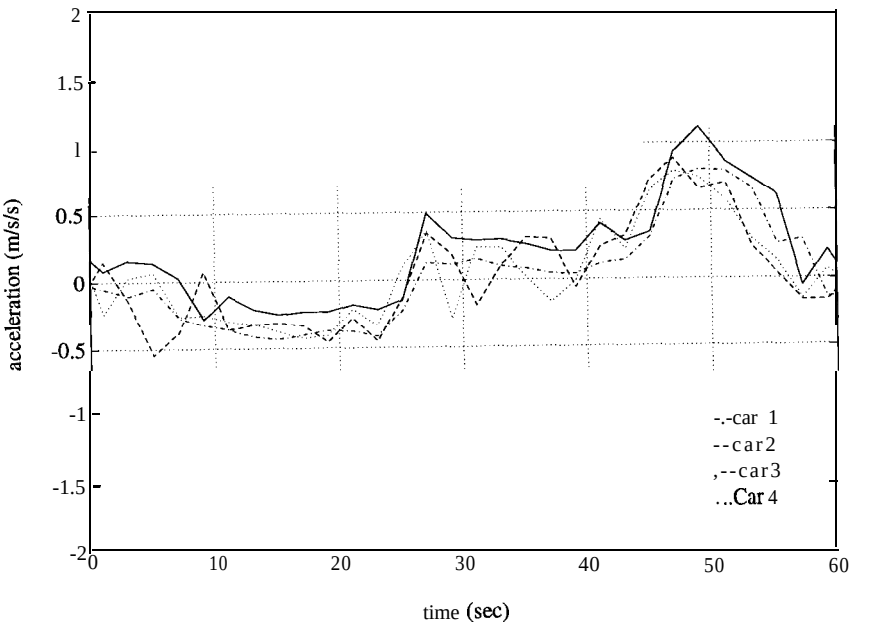

Figure 3 1c: Four car platoon accelerations: Variable velocity profile.

Chapter 7
Conclusions

Simulation results have shown that longitudinal controllers based on the non-linear techniques, sliding controls and/or Input-Output Linearization, can be used in a multiple vehicle following configuration. The spacing based controllers can also eliminate amplification of successive spacing errors from the platoon control problem. It was shown, however, that the constant headway controllers did not satisfactorily solve the control task. These controllers resulted in larger control action and consequently deteriorated ride quality, as compared to the spacing-based controllers.

The successful operation of the IPCS demonstrated the feasibility of using current technology for this application. It must be noted that this implementation was conducted using four vehicles. For larger platoon sizes, it remains to be seen if simulation results are correct in predicting that platoon-stability will be maintained.

There are several improvements being made in the IPCS. The radar system is being replaced by VORAD Safety Systems Inc. with a digital radar system. The radar range measurements will be improved in accuracy and in the capability to provide reliable separation distances at low closing rates.

Four car platoon testing will be continue as part of the next phase of these experiments. At that time the IPCS will be utilizing the improved system units. Also, as part of the next phase of experimental testing, the use of brake control under moderate as well as emergency situations will be investigated. Due to the inadequacy of the current pneumatic brake actuation system it is being replaced by a hydraulic brake actuation system.

Acknowledgement

The research reported herein is a part of the Partners for Advanced Transit and Highways (PATH), performed under the sponsorship of the State of California Business, Transportation, and Housing Agency, Department of Transportation; and the U.S. Department of Transportation, Federal Highway Administration.

References

[1] Bender, J. G., "An Overview if Systems Studies of Automated Highway Systems", ***IEEE Trans. on Vehicular Technology,*** Feb. 1991.

[2] Caudill, R. J., and Garrard, W.L., "Vehicle-Follower Longitudinal Control for Automated Transit Vehicles", Transactions ASME ***Journal of Dynamic Systems, Measurement, and Control,*** Vol. 99, December 1977, pp. 241-248,

[3] Chang, K. S., et al., "Experimentation with a Vehicle Platoon Control System", ***Proceedings of the 1991 Vehicle Navigation and Information Systems Conference,*** Dearborn, MI.

[4] Cho, D., and Hedrick, J. K., 1989a, "Automotive Powertrain Modeling for Control", Transactions ASME ***Journal of Dynamic Systems, Measurement, and Control,*** Vol. 111, No. 4, December.

[5] Garrard, W. L., Caudill, R. J., Kornhauser, A. L., MacKinnon, D., and Brown, S. J., 1978, "State-of-the-Art of Longitudinal Guideway Transit Vehicles", ATA ***Journal of Advanced Transportation,*** Vol. 12, pp. 35-67.

[6] Green, J., and Hedrick, J. K., 1990, "Nonlinear Torque Control for Gasoline Engines", ***Proceedings of the 1990 American Control Conference,*** San Diego, CA.

[7] Hedrick, J. K., McMahon, D. H., Narendran, V. K., and Swaroop, D., 1991, "Longitudinal Vehicle Controller Design for IVHS Systems", ***Proceedings of the 1991 American Control Conference,*** Boston, MA.

[8] McMahon, D. H., Hedrick, J. K., and Shladover, S. E., 1990, "Vehicle Modeling and Control for Automated Highway Systems", ***Proceedings of the 1990 American Control Conference, San*** Diego, CA.

[9] Moskwa, J. J., and Hedrick, J. K., 1989a, "Modeling and Validation of Automotive Engines for Control Algorithm Development", ASME WAM, ***Advanced***

Automotive Technologies -1989, DSC-Vol. 13, Ed. Karmel, A. M., et al.

[10] Shigley, J. E., and Mischke, C.R., ***Mechanical Engineering Design,*** McGraw Hill Publishing Co., 1989.

[11] Shladover, S., et al., "Automated Vehicle Control Developments in the PATH Program", ***IEEE Trans. on Vehicular Technology,*** Feb. 1991.

[12] Shladover, S., "Dynamic Entrainment of automated Guidway Transit Vehi***cles", High Speed Ground Transportation Journal,*** Vol. 12, No. 3, Fall 1978, pp 87-l 13.

[13] White, A. J., ***Brake Dynamics: An Introduction to Vehicle Brake Testing at the Inspection Station Level",*** Motor Vehicle Research of New Hampshire, 1963.a

[14] Wong, J. ***Y., Theory of Ground Vehicles,*** John Wiley & Sons, 1978.